

Domain Decomposition Learning Methods for Solving Elliptic Problems

Qi Sun*, Xuejun Xu^{*,†}, and Haotian Yi*

Abstract. With the aid of hardware and software developments, there has been a surge of interests in solving partial differential equations by deep learning techniques, and the integration with domain decomposition strategies has recently attracted considerable attention due to its enhanced representation and parallelization capacity of the network solution. While there are already several works that substitute the numerical solver of overlapping Schwarz methods with the deep learning approach, the non-overlapping counterpart has not been thoroughly studied yet because of the inevitable interface overfitting problem that would propagate the errors to neighbouring subdomains and eventually hamper the convergence of outer iteration. In this work, a novel learning approach, *i.e.*, the compensated deep Ritz method, is proposed to enable the flux transmission across subregion interfaces with guaranteed accuracy, thereby allowing us to construct effective learning algorithms for realizing the more general non-overlapping domain decomposition methods in the presence of overfitted interface conditions. Numerical experiments on a series of elliptic boundary value problems including the regular and irregular interfaces, low and high dimensions, smooth and high-contrast coefficients on multidomains are carried out to validate the effectiveness of our proposed domain decomposition learning algorithms.

Key words. neural networks, domain decomposition methods, elliptic partial differential equations, boundary overfitting, compensated deep Ritz method.

AMS subject classifications. 65M55, 65Nxx, 92B20, 49S05.

1. Introduction. Many problems of interested in science and engineering are modelled by partial differential equations, which help us understand and control complex systems across a wide variety of real-world applications [10]. Unfortunately, it is often difficult or impossible to obtain their analytical solutions, therefore various numerical techniques including, but not limited to the finite difference, finite volume, and finite element methods [27, 28, 5] have been developed to obtain their approximate solutions. Based on a discretization of the solution space by dividing the computational domain into a polygon mesh, these numerical methods are highly accurate and efficient for low-dimensional problems on regular domains. However, there are still many challenging issues to be addressed, *e.g.*, mesh generation remains complex when the boundary is geometrically complicated or dynamically changing, computation of high-dimensional problems is often infeasible due to the so-called curse of dimensionality, and many others. As the traditional methods are continuously being improved, it also raises the need for new methods and tools in order to tackle the difficulties mentioned above [23].

With the significant enhancement of hardware and software developments, the deep learning methods [26] have recently emerged as an attractive alternative for solving different types of equations in both the forward and inverse problems [43, 13, 6], and have achieved remarkable success due to the universal approximation [40] of neural networks as an ansatz to the

*School of Mathematical Sciences, Tongji University, Shanghai 200092, China (qsun_irl@tongji.edu.cn, 2111166@tongji.edu.cn).

†Institute of Computational Mathematics, AMSS, Chinese Academy of Sciences, Beijing 100190, China (xxj@lsec.cc.ac.cn).

solution function or the operator mapping [23]. For instance, one of the most representative work is the physics-informed neural network (PINN) [39, 25, 24], where the differential operators can be exactly calculated via automatic differentiation [37] and the residual of the governing equations is incorporated into the training loss function. Another pioneering work is the deep Ritz method [47], which resorts to the variational principle and performs better for problems with low-regularity solutions [7]. It is also possible to design the training task that is corresponded to the weak formulation of the underlying equations [48], but the training process is often hard to converge due to the imbalance between generative and adversarial networks. Furthermore, to make the trained model satisfy the boundary conditions as precise as possible, various techniques including, but not limited to the deep Nitsche method [32], the augmented Lagrangian relaxation [20], and the auxiliary network with distance function [34, 3] have been developed. When compared with the traditional numerical solvers [27, 5], these deep learning methods enjoy advantages of flexible and meshless implementation, strong ability to tackle non-linearity and to break the curse of dimensionality, and others [23]. However, they may still exhibit poor performance in handling problems with multi-scale phenomena [46, 21], and the large training cost is also a major drawback that limits their application in the field of large-scale scientific computing. To further enhance the representation and parallelization capacity of the network solution, it is natural to integrate the state-of-the-art deep learning techniques with the conventional domain decomposition strategies [17], aiming at paving the way for truly enabling the large-scale computation using neural networks.

One way is to incorporate the distributed training techniques [2], *e.g.*, the data and module parallelization, into the PINN approach [21, 22, 19], where the training task is split into multiple subproblems according to the non-overlapping partition of domain and simple continuity conditions are enforced across the subregion interfaces. Although this combination is quite general and parallelizable, no specific knowledge of the underlying problem is utilized during the training process, which substantially differs from the conventional methodology of splitting a partial differential equation [45, 38]. On the other hand, as the classical domain decomposition methods [45] can be formulated at the continuous or the weak level, various works have been devoted to employing the learning approaches for solving the decomposed subproblems and therefore benefit from the mesh free nature of deep learning solvers. Under such circumstances, the machine learning analogue of the overlapping domain decomposition methods have emerged recently and have successfully handled many problems [32, 29, 35, 42], however, the more general non-overlapping counterpart has not been thoroughly studied yet. A major difficulty is that the network solutions of local problems are prone to overfitting at and near the interface [9, 1] since the interface conditions are enforced as soft penalty functions during training and the size of training data on interface is smaller than that of interior domains, which eventually propagates the errors to neighboring subdomains and hampers the convergence of outer iteration. In other words, the issue of boundary overfitting is a key threat to the integration of deep learning techniques and domain decomposition methods, especially for those based on a direct flux exchange across the subdomain interfaces. What's worse, it will always occur to a greater or lesser extent in practical implementations and has not been fully addressed or studied in the existing literature.

In this work, we consider the benchmark Poisson equation that serves as a necessary prerequisite to validate the effectiveness of the domain decomposition learning approaches

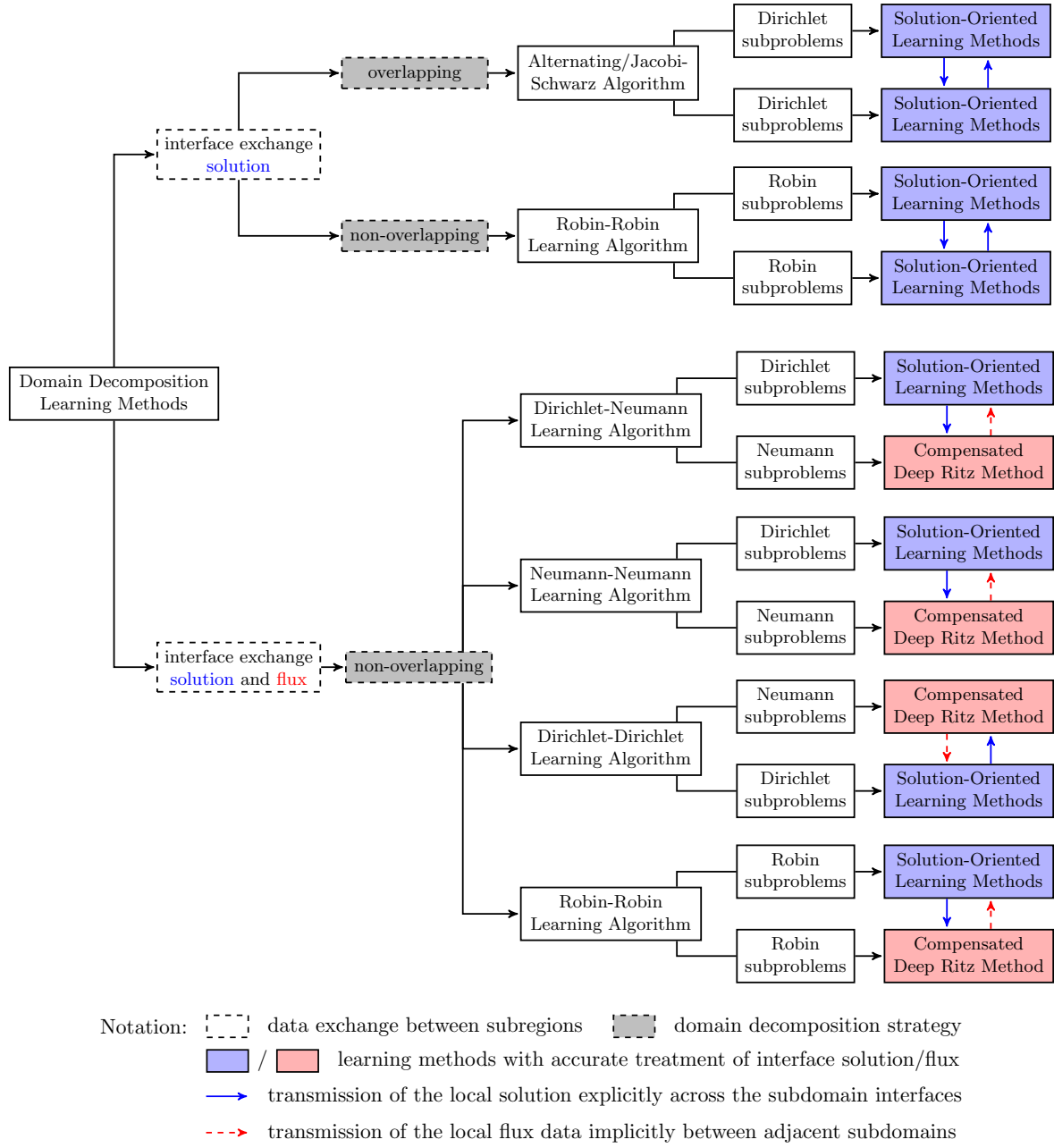


Figure 1: Our proposed framework of domain decomposition learning methods for solving the elliptic boundary value problems.

[29, 30, 35], namely,

$$(1.1) \quad \begin{aligned} -\Delta u(x) &= f(x) && \text{in } \Omega, \\ u(x) &= 0 && \text{on } \partial\Omega, \end{aligned}$$

where $d \in \mathbb{N}_+$ is the dimension, $\Omega \subset \mathbb{R}^d$ a bounded domain, and $f(x) \in L^2(D)$ a given function. Note that for the case of inhomogeneous boundary conditions, it is equivalent to solving (1.1) after employing an auxiliary network with distance function for boundary fitting [34, 3]. In contrast to the standard classification of domain decomposition methods that are based on the partition strategy of the computational domain, our proposed framework (see Figure 1) is established on the information exchange across the subdomain interfaces. More specifically, with the set of interface points being small compared to the entire training dataset, the trained models are often found to satisfy the governing equations but for overfitted interface conditions [9]. As a direct result, though the solution value of local problem is often found to be of satisfactory accuracy in both the interior and boundary points, the flux prediction through trained models is typically of unacceptable low accuracy along the interface and therefore hampers the convergence of direct flux exchange schemes. For simplicity, we refer to these deep learning solvers as the solution-oriented learning methods [39, 47] in what follows, since the issue of boundary overfitting will always occur to a greater or lesser extent in practice. To deal with the overfitted interface conditions, we propose a novel learning approach, *i.e.*, the compensated deep Ritz method, that allows the accurate flux transmission between neighbouring subdomains but without explicitly computing the solution's derivatives on the interface. Thanks to the proposed method, we are now able to construct effective learning approaches for realizing the classical Dirichlet-Neumann, Neumann-Neumann, Dirichlet-Dirichlet, and Robin-Robin algorithms in the non-overlapping regime [45] (see Figure 1), and experimental results conducted on a series of elliptic boundary value problems validate our statements. It is noteworthy that although the Robin-Robin algorithm only requires the exchange of solution value across the interfaces [8], two additional parameters in the Robin boundary conditions need to be determined and may lead to interface overfitting if not chosen appropriately. Fortunately, our compensated deep Ritz method can also help to alleviate this problem.

The remainder of this paper is organized as follows. In section 2, we present a brief review of the classical domain decomposition methods and the solution-oriented learning methods for solving elliptic boundary value problems. Then, according to our framework (see Figure 1), the most straightforward machine learning analogue of the Robin-Robin algorithm is introduced in section 3, followed by the detailed illustration of our compensated deep Ritz method in section 4. Numerical experiments on a series of problems including the regular and irregular interfaces, two and four subdomains, low and high dimensions are reported in section 5, as well as the more challenging elliptic interface problem with high-contrast coefficients. Section 6 will conclude this paper and present some directions for future work.

2. Preliminaries. This section is devoted to briefly reviewing the classical domain decomposition methods [45, 38] and the widely-used deep learning methods for solving the second-order elliptic boundary value problems.

2.1. Domain Decomposition Methods. The idea of domain decomposition for solving the Poisson equation has a long history dating back to the 18th century [41], and there is a vast literature on domain decomposition methods (we refer to [45, 38, 33] and the references cited therein). For the ease of illustration, the computational domain $\Omega \subset \mathbb{R}^d$ is first assumed to be partitioned into two subdomains $\{\Omega_i\}_{i=1}^2$ (see Figure 2 for example), while the case of multiple subdomains can be obtained in a similar way. Depending on the partition strategies being

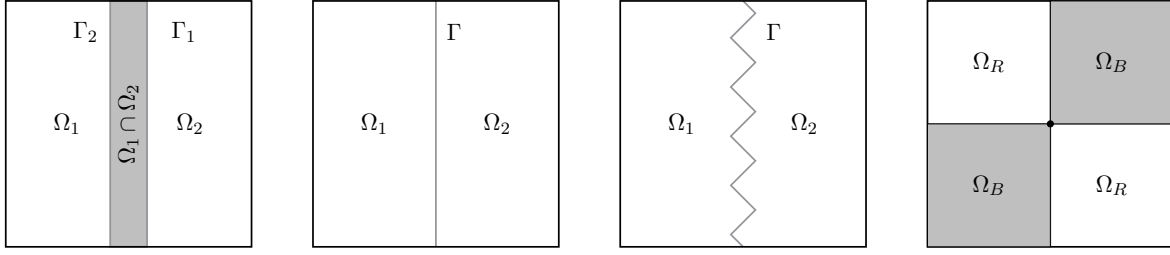


Figure 2: Decomposition of a bounded domain $\Omega \subset \mathbb{R}^2$ in two dimension. **Left:** Overlapping partition with two subdomains. **Middle:** Non-overlapping partition with two subdomains, which is separated by curved regular or irregular interfaces. **Right:** Red-Black partition of the non-overlapping multidomains into two sets, where the intersection between two subregions in the same class is marked in bold.

employed, the domain decomposition methods are typically categorized into the overlapping and non-overlapping groups, which poses no problem if the finite difference or finite element methods are utilized as the numerical solvers for local problems [45, 38].

However, when the neural network is adopted as the solution ansatz, the trained model is often found to satisfies the governing equations but for overfitted boundary conditions [9, 1], which greatly differs from the traditional methods [45, 38]. To this end, the classification of domain decomposition methods adopted in this paper is based on the information exchange between neighbouring subregions (see also Figure 1). More specifically, we summarize in what follows some representative decomposition-based approaches in the literature [45]. Here, we refer to the Schwarz alternating method and the Robin-Robin algorithm as SAM and RRA in algorithm 2.1, while the Dirichlet-Neumann, Neumann-Neumann, and Dirichlet-Dirichlet algorithms are abbreviated as DNA, NNA, and DDA in algorithm 2.2, respectively. In addition, the relaxation parameter ρ shall lay between $(0, \rho_{max})$ in order to achieve convergence [11]. Notably, although the overlapping methods with small overlap are cheap and easy to implement, it comes at the price of slower convergence. Besides, the non-overlapping methods are more efficient in handling elliptic problems with large jumps in the coefficients.

2.2. Deep Learning Solvers. As can be concluded from the previous discussion, the decomposed problem on each subregion takes on the following form

$$(2.1) \quad \begin{aligned} -\Delta u_i(x) &= f(x) && \text{in } \Omega_i, \\ u_i(x) &= 0 && \text{on } \partial\Omega_i \setminus \Gamma, \\ \mathcal{B}_i u_i(x) &= h_i(x) && \text{on } \Gamma, \end{aligned}$$

where \mathcal{B}_i is a boundary operator on interface that may represent the Dirichlet, Neumann, or Robin boundary condition, namely,

$$\begin{aligned} \text{Dirichlet condition:} \quad & \mathcal{B}_i u(x) = u(x), \\ \text{Neumann condition:} \quad & \mathcal{B}_i u(x) = \nabla u(x) \cdot \mathbf{n}_i, \\ \text{Robin condition:} \quad & \mathcal{B}_i u(x) = \nabla u(x) \cdot \mathbf{n}_i + \kappa_i u(x), \end{aligned}$$

and the associated boundary conditions $h_i(x)$ are iteratively determined so as to ensure the transmission conditions across subdomain interfaces [45].

Algorithm 2.1 Domain Decomposition Methods Based on Solution Exchange

Start with the initial guess $h_1^{[0]}$ and $h_2^{[0]}$ of each subsolution along the interface;
for $k \leftarrow 0$ to K (maximum number of outer iterations) **do**
 while stopping criteria are not satisfied **do**
 % *Local Problem-Solving*

$$\begin{cases} -\Delta u_1^{[k]} = f & \text{in } \Omega_1 \\ u_1^{[k]} = 0 & \text{on } \partial\Omega_1 \setminus \Gamma_1 \\ \mathcal{B}_1 u_1^{[k]} = h_1^{[k]} & \text{on } \Gamma_1 \end{cases} \quad \text{where } \mathcal{B}_1 u_1^{[k]} = \begin{cases} u_1^{[k]} & \text{(SAM)} \\ \nabla u_1^{[k]} \cdot \mathbf{n}_1 + \kappa_1 u_1^{[k]} & \text{(RRA)} \end{cases}$$

 % *Solution Exchange Between Subdomains*

$$h_2^{[k]} = \begin{cases} u_1^{[k]} & \text{on } \Gamma_2 \quad \text{(SAM)} \\ -h_1^{[k]} + (\kappa_1 + \kappa_2)u_1^{[k]} & \text{on } \Gamma_2 \quad \text{(RRA)} \end{cases}$$

 % *Local Problem-Solving*

$$\begin{cases} -\Delta u_2^{[k]} = f & \text{in } \Omega_2 \\ u_2^{[k]} = 0 & \text{on } \partial\Omega_2 \setminus \Gamma_2 \\ \mathcal{B}_2 u_2^{[k]} = h_2^{[k]} & \text{on } \Gamma_2 \end{cases} \quad \text{where } \mathcal{B}_2 u_2^{[k]} = \begin{cases} u_2^{[k]} & \text{(SAM)} \\ \nabla u_2^{[k]} \cdot \mathbf{n}_2 + \kappa_2 u_2^{[k]} & \text{(RRA)} \end{cases}$$

 % *Solution Exchange Between Subdomains*

$$h_1^{[k+1]} = \begin{cases} u_2^{[k]} & \text{on } \Gamma_1 \quad \text{(SAM)} \\ \rho + (1 - \rho)(-h_2^{[k]} + (\kappa_1 + \kappa_2)u_2^{[k]}) & \text{on } \Gamma_1 \quad \text{(RRA)} \end{cases}$$

 end while
end for

Remark: RRA is defined in the non-overlapping regime, *i.e.*, $\Gamma_1 = \Gamma_2$ during iteration.

When the deep learning techniques are employed for solving the boundary value problem (2.1), the hypothesis space of local solution is first built by neural networks. Here, we adopt the standard fully-connected neural network of depth $L \in \mathbb{N}_+$ [18], in which the ℓ -th hidden layer receives an input $x^{\ell-1} \in \mathbb{R}^{n_{\ell-1}}$ from its previous layer and transforms it to

$$T^\ell(x^{\ell-1}) = \mathbf{W}^\ell x^{\ell-1} + \mathbf{b}^\ell,$$

where $\mathbf{W}^\ell \in \mathbb{R}^{n_\ell \times n_{\ell-1}}$ and $\mathbf{b}^\ell \in \mathbb{R}^{n_\ell}$ are the weights and biases to be learned. By choosing an appropriate activation function $\sigma(\cdot)$ for each hidden layer, the network solution can then be defined as

$$\hat{u}_i(x; \theta) = (T^L \circ \sigma \circ T^{L-1} \cdots \circ \sigma \circ T^1)(x),$$

where \circ represents the composition operator and $\theta = \{\mathbf{W}^\ell, \mathbf{b}^\ell\}_{\ell=1}^L$ denotes the collection of the trainable parameters. One can also employ other network architectures, *e.g.*, the residual

Algorithm 2.2 Domain Decomposition Methods Based on Solution and Flux Exchange

Start with the initial guess $h_1^{[0]}$ and $h_2^{[0]}$ of each subsolution along the interface;

for $k \leftarrow 0$ to K (maximum number of outer iterations) **do**

while stopping criteria are not satisfied **do**

 % *Local Problem-Solving*

$$\begin{cases} -\Delta u_i^{[k]} = f & \text{in } \Omega_i \\ u_i^{[k]} = 0 & \text{on } \partial\Omega_i \setminus \Gamma \\ \mathcal{B}_i u_i^{[k]} = h_i^{[k]} & \text{on } \Gamma \end{cases} \quad \text{where } \mathcal{B}_i u_i^{[k]} = \begin{cases} u_i^{[k]} & \text{for } i = 1, \quad (\text{DNA}) \\ u_i^{[k]} & \text{for } i = 1, 2, \quad (\text{NNA}) \\ \nabla u_i^{[k]} \cdot \mathbf{n}_i & \text{for } i = 1, 2, \quad (\text{DDA}) \end{cases}$$

 % *Solution or Flux Exchange Between Subdomains*

$$h_i^{[k]} = \begin{cases} -\nabla u_{i-1}^{[k]} \cdot \mathbf{n}_{i-1} & \text{on } \Gamma \text{ for } i = 2, \quad (\text{DNA}) \\ \nabla u_1^{[k]} \cdot \mathbf{n}_1 + \nabla u_2^{[k]} \cdot \mathbf{n}_2 & \text{on } \Gamma \text{ for } i = 1, 2, \quad (\text{NNA}) \\ u_1^{[k]} - u_2^{[k]} & \text{on } \Gamma \text{ for } i = 1, 2, \quad (\text{DDA}) \end{cases}$$

 % *Local Problem-Solving*

$$\begin{cases} -\Delta u_i^{[k]} = f & \text{in } \Omega_i \\ u_i^{[k]} = 0 & \text{on } \partial\Omega_i \setminus \Gamma \\ \mathcal{B}_i u_i^{[k]} = h_i^{[k]} & \text{on } \Gamma \end{cases} \quad \text{where } \mathcal{B}_i u_i^{[k]} = \begin{cases} \nabla u_i^{[k]} \cdot \mathbf{n}_i & \text{for } i = 2, \quad (\text{DNA}) \\ \nabla u_i^{[k]} \cdot \mathbf{n}_i & \text{for } i = 1, 2, \quad (\text{NNA}) \\ u_i^{[k]} & \text{for } i = 1, 2, \quad (\text{DDA}) \end{cases}$$

 % *Solution or Flux Exchange Between Subdomains*

$$h_i^{[k+1]} = \begin{cases} \rho u_{i+1}^{[k]} + (1 - \rho) u_i^{[k]} & \text{on } \Gamma \text{ for } i = 1, \quad (\text{DNA}) \\ h_i^{[k]} - \rho(u_1^{[k]} + u_2^{[k]}) & \text{on } \Gamma \text{ for } i = 1, 2, \quad (\text{NNA}) \\ h_i^{[k]} - \rho(\nabla u_1^{[k]} \cdot \mathbf{n}_1 + \nabla u_2^{[k]} \cdot \mathbf{n}_2) & \text{on } \Gamma \text{ for } i = 1, 2, \quad (\text{DDA}) \end{cases}$$

end while

end for

network and its variants [15, 13], for the parametrization of local solutions, which is omitted here and left for future investigation.

To update the trainable parameters through the celebrated backpropagation algorithm [16], various training loss functions (before employing the numerical integration) have been proposed, *e.g.*, the PINN approach [39] that is based on the strong form of (2.1), namely,

$$\hat{u}_i(x; \theta) = \arg \min_{\theta} \int_{\Omega_i} |-\Delta \hat{u}_i - f|^2 dx + \beta \left(\int_{\partial\Omega_i \setminus \Gamma} |\hat{u}_i|^2 ds + \int_{\Gamma} |\mathcal{B}_i(\hat{u}_i) - h_i|^2 ds \right),$$

or the deep Ritz method [47] that is based on the variational form of (2.1), namely,

$$\hat{u}_i(x; \theta) = \arg \min_{\theta} \int_{\Omega_i} \left(\frac{1}{2} |\nabla \hat{u}_i|^2 - f \hat{u}_i \right) dx + \beta \int_{\partial\Omega_i \setminus \Gamma} |\hat{u}_i|^2 ds + L_{\Gamma}(\hat{u}_i(x; \theta))$$

where the last term depends on the boundary condition being imposed at the interface

$$L_{\Gamma}(\hat{u}_i(x; \theta)) = \begin{cases} \beta \int_{\Gamma} |\hat{u}_i - h_i|^2 ds & \text{(Dirichlet condition),} \\ - \int_{\Gamma} h_i \hat{u}_i ds & \text{(Neumann condition),} \\ \int_{\Gamma} \left(\frac{\kappa_i}{2} |\hat{u}_i|^2 - h_i \hat{u}_i \right) ds & \text{(Robin condition),} \end{cases}$$

and $\beta > 0$ is a user-defined penalty coefficient.

Apart from these two widely-used methods, the weak adversarial network [48] is based on the weak form of (2.1), while another series of neural network methods is designed to use separate networks to fit the interior and boundary equations respectively [34, 3]. We refer the readers to [23, 42, 17] for a more detailed review of the existing deep learning solvers. Notably, with the interface conditions being included as soft constraints in the training loss function and the set of interface points being small compare to that of interior domains, the trained network is highly prone to overfitting at the interface [9, 1], which is a key threat to the integration of the direct flux exchange schemes and the deep learning techniques but rarely studied or addressed in the literature.

3. Robin-Robin Algorithm via Solution-Oriented Learning Methods. Note that in addition to the deep learning analogue of overlapping Schwarz methods [29, 35, 30, 42, 44], the non-overlapping Robin-Robin algorithm [45, 38] is also based on a direct exchange of solution value between neighbouring subdomains (see Figure 1 or algorithm 2.1). Moreover, as the decomposition leads to simpler and smoother functions to be learned on each subregion, it thus enables us to employ the standard solution-oriented learning methods [39, 47, 48, 43] for the numerical solution of local problems. As such, the PINN approach [39] is generally preferred since it is known to empirically work better for problems with smooth solutions [7]. However, a major drawback is the determination of two additional parameters in the Robin boundary conditions, which may cause difficulties for network training or require more outer iterations to converge.

For the ease of illustration, we consider the case of two non-overlapping subregions (see Figure 2) in what follows, where the interface conditions are invariably of the Robin type [45, 38, 8]. Note that the detailed iterative process in terms of differential operators is presented in algorithm 2.1, which is not restated here for simplicity. It can be observed that the update of interface conditions only requires the Dirichlet data of local solutions, which seems simpler and more straightforward than those based on a direct flux exchange [45, 38] when combining with the deep learning models.

To realize the Robin-Robin algorithm using the PINN approach, the local problem is first rewritten as an equivalent optimization problem by minimizing the residual of the governing equation, namely, for $i = 1, 2$,

$$(3.1) \quad u_i^{[k]} = \arg \min_{u_i \in V_i} \int_{\Omega_i} |-\Delta u_i - f|^2 dx + \beta \left(\int_{\Gamma} \left| \kappa_i u_i + \frac{\partial u_i}{\partial \mathbf{n}_i} - h_i^{[k]} \right|^2 ds + \int_{\partial\Omega \cap \partial\Omega_i} |u_i|^2 ds \right),$$

where the boundary and interface conditions are included as soft penalty terms in the training

Algorithm 3.1 Deep Learning Analogue of Robin-Robin Algorithm for Two Subdomains

```

% Initialization
– divide domain  $\Omega \subset \mathbb{R}^d$  into two non-overlapping subregions  $\Omega_1$  and  $\Omega_2$ ;
– specify network structures  $\hat{u}_1(x; \theta_1)$  and  $\hat{u}_2(x; \theta_2)$  for each subproblem;
– generate Monte Carlo training samples  $X_\Gamma$ ,  $X_{\Omega_i}$ , and  $X_{D_i}$  for  $i = 1, 2$ ;
% Outer Iteration Loop
Start with the initial guess  $h^{[0]}$  along the interface  $\Gamma$ ;
for  $k \leftarrow 0$  to  $K$  (maximum number of outer iterations) do
  while stopping criteria are not satisfied do
    % Robin Subproblem-Solving via Solution-Oriented Learning Method
    for  $\ell \leftarrow 0$  to  $L$  (maximum number of training epochs) do
      for  $m \leftarrow 0$  to  $M$  (maximum number of training mini-batches) do
        – draw mini-batch data uniformly at random from  $X_\Gamma$ ,  $X_{\Omega_1}$ , and  $X_{D_1}$ ;
        – network training by employing solution-oriented learning method (3.2), i.e.,
          
$$\theta_1^{[k]} = \arg \min_{\theta_1} L_{\Omega_1}(\hat{u}_1) + \beta \left( L_{D_1}(\hat{u}_1) + L_R(\hat{u}_1, h_1^{[k]}) \right)$$

      end for
    end for
    % Update of boundary values at interface  $\Gamma$ 
    for  $n \leftarrow 1$  to  $N_\Gamma$  do
      
$$h_2^{[k]}(x_n^\Gamma) = -h_1^{[k]}(x_n^\Gamma) + (\kappa_1 + \kappa_2)\hat{u}_1(x_n^\Gamma; \theta_1^{[k]})$$

    end for
    % Robin Subproblem-Solving via Solution-Oriented Learning Method
    for  $\ell \leftarrow 0$  to  $L$  (maximum number of training epochs) do
      for  $m \leftarrow 0$  to  $M$  (maximum number of training mini-batches) do
        – draw mini-batch data uniformly at random from  $X_{\Omega_1}$ ,  $X_{\Omega_2}$ ,  $X_{D_1}$ , and  $X_{D_2}$ ;
        – network training by employing solution-oriented learning method (3.2), i.e.,
          
$$\theta_2^{[k]} = \arg \min_{\theta_2} L_{\Omega_2}(\hat{u}_2) + \beta \left( L_{D_2}(\hat{u}_2) + L_R(\hat{u}_2, h_2^{[k]}) \right)$$

      end for
    end for
    % Update of boundary values at interface  $\Gamma$ 
    for  $n \leftarrow 1$  to  $N_\Gamma$  do
      
$$h_1^{[k+1]}(x_n^\Gamma) = \rho h_1^{[k]}(x_n^\Gamma) + (1 - \rho)(-h_2^{[k]}(x_n^\Gamma) + (\kappa_1 + \kappa_2)\hat{u}_2(x_n^\Gamma; \theta_2^{[k]}))$$

    end for
  end while
end for

```

loss function. Then, by parametrizing the trial functions as neural networks

$$u_1^{[k]}(x) \approx \hat{u}_1^{[k]}(x) := \hat{u}_1(x; \theta_1^{[k]}) \quad \text{and} \quad u_2^{[k]}(x) \approx \hat{u}_2^{[k]}(x) := \hat{u}_2(x; \theta_2^{[k]}),$$

and generating the training sample points inside each subregion and at its boundary, *i.e.*,

$$X_{\Omega_i} = \{x_n^{\Omega_i}\}_{n=1}^{N_{\Omega_i}}, \quad X_{D_i} = \{x_n^{D_i}\}_{n=1}^{N_{D_i}}, \quad \text{and} \quad X_{\Gamma} = \{x_n^{\Gamma}\}_{n=1}^{N_{\Gamma}},$$

the powerful stochastic optimization tools [4] can be applied for fulfilling the learning tasks associated with (3.1), that is, for $i = 1, 2$ and the k -th outer iteration,

$$(3.2) \quad \theta_i^{[k]} = \arg \min_{\theta_i} L_{\Omega_i}(\hat{u}_i(x; \theta_i)) + \beta \left(L_{D_i}(\hat{u}_i(x; \theta_i)) + L_R(\hat{u}_i(x; \theta_i), h_i^{[k]}(x)) \right),$$

where the loss functions (not relabelled) are defined as

$$\begin{aligned} L_{\Omega_i}(\hat{u}_i(x; \theta_i)) &= \frac{|\Omega_i|}{N_{\Omega_i}} \sum_{n=1}^{N_{\Omega_i}} |\Delta \hat{u}_i(x_n^{\Omega_i}; \theta_i) - f(x_n^{\Omega_i})|^2, \\ L_{D_i}(\hat{u}_i(x; \theta_i)) &= \frac{|\partial\Omega_i \setminus \Gamma|}{N_{D_i}} \sum_{n=1}^{N_{D_i}} |\hat{u}_i(x_n^{D_i}; \theta_i)|^2, \\ L_R(\hat{u}_i(x; \theta_i), h_i^{[k]}(x)) &= \frac{|\Gamma|}{N_{\Gamma}} \sum_{n=1}^{N_{\Gamma}} \left| \kappa_i \hat{u}_i(x_n^{\Omega_i}; \theta_i) + \frac{\partial \hat{u}_i}{\partial \mathbf{n}_i}(x_n^{\Omega_i}; \theta_i) - h_i^{[k]}(x_n^{\Omega_i}) \right|^2. \end{aligned}$$

Here, and in what follows, $|\Omega_i|$, $|\partial\Omega_i \setminus \Gamma|$, and $|\Gamma|$ denote the Jacobians of the transformations that map the random variables generated from a standard uniform distribution to the input sample points X_{Ω_i} , X_{D_i} , and X_{Γ} , respectively, where $i = 1, 2$.

To sum up, by employing the standard PINN approach as the numerical solver of local problems, the deep learning analogue of the classical Robin-Robin algorithm is presented in Algorithm 3.1, where $\kappa_1, \kappa_2 > 0$ are two additional user-defined parameters. We can assume, without loss of generality, that $\kappa_1 = 1$ and leave the other parameter to be tuned. In fact, as the size of the training data on interfaces is typically much smaller than that of interior domains, too large (or small) value of $\kappa_2 > 0$ may cause weights imbalance in the training loss function and hence make the training process susceptible to overfitting on the interface, while a moderate value can guarantee convergence but at the cost of more outer iterations. This greatly differs from the conventional finite element setting [8] since the neural network is adopted as the solution ansatz, and is further demonstrated through numerical experiments in section 5. Fortunately, the issue of weights imbalance can be tackled by using our compensated deep Ritz method, which is theoretically and numerically studied in the following sections.

4. Compensated Deep Ritz Method. In this section, we begin by focusing on the non-overlapping domain decomposition methods that are based on the direct flux exchange between neighbouring subregions (see Figure 1). When solving the decomposed problems using neural networks, it is known that although the overall training loss tends to be decreased as the iteration proceeds, the trained model often converges to a local minimizer that adequately satisfies the constrained equations but for overfitted boundary conditions [9, 1]. In other words, the flux approximation using trained networks is typically of unacceptable low accuracy at and near the interface, preventing us from deploying the solution-oriented learning methods [39, 47] for solving the decomposed subproblems.

To overcome such an inevitable drawbacks in practical situations, the compensated deep Ritz method is proposed to enable the accurate transmission of numerical flux in the presence of overfitted interface conditions, which is of key importance for developing the effective Dirichlet-Neumann, Neumann-Neumann, and Dirichlet-Dirichlet learning algorithms. Moreover, it can also help to alleviate the issue of interface overfitting when realizing the Robin-Robin algorithm through deep learning techniques. Consequently, we will be able to fully leverage the benefits of deep learning solvers to deal with the complicated geometry domains, high-dimensional problems, and many others [23].

4.1. Dirichlet-Neumann Learning Algorithm. We begin by considering the Dirichlet-Neumann algorithm [45, 38], where the detailed iterative process in terms of differential operators is presented in Algorithm 2.2. To avoid the explicit computation and transmission of interface flux, the variational formulation of the multidomain problem is taken into consideration. More precisely, by integrating by parts in $\Omega \subset \mathbb{R}^d$, the weak formulation of the Poisson equation (1.1) reads: find $u \in H_0^1(\Omega)$ such that

$$(4.1) \quad a(u, v) = (f, v) \quad \text{for any } v \in H_0^1(\Omega),$$

where the bilinear forms are defined as

$$a(u, v) = \int_{\Omega} \nabla u \cdot \nabla v \, dx \quad \text{and} \quad (f, v) = \int_{\Omega} f v \, dx.$$

For the ease of illustration, we consider a two subdomain decomposition of (4.1) in what follows, and similar results can be achieved for multidomain problems using a red-black partition [45]. Under such a circumstance, let Ω_1, Ω_2 denote a non-overlapping decomposition of domain $\Omega \subset \mathbb{R}^d$, with interface $\Gamma = \partial\Omega_1 \cap \partial\Omega_2$ separating the subregions (see Figure 2 for example). By defining the bilinear terms

$$a_i(u_i, v_i) = \int_{\Omega_i} \nabla u_i \cdot \nabla v_i \, dx \quad \text{and} \quad (f, v_i)_i = \int_{\Omega_i} f v_i \, dx$$

and setting

$$V_i = \{v_i \in H^1(\Omega_i) \mid v_i|_{\partial\Omega \cap \partial\Omega_i} = 0\} \quad \text{and} \quad V_i^0 = H_0^1(\Omega_i)$$

for $i = 1, 2$, the Green's formula then implies that (4.1) can be equivalently reformulated as: find $u_1 \in V_1$ and $u_2 \in V_2$ such that

$$\begin{aligned} a_1(u_1, v_1) &= (f, v_1)_1 && \text{for any } v_1 \in V_1^0, \\ u_1 &= u_2 && \text{on } \Gamma, \\ a_2(u_2, v_2) &= (f, v_2)_2 + (f, R_1 \gamma_0 v_2)_1 - a_1(u_1, R_1 \gamma_0 v_2) && \text{for any } v_2 \in V_2, \end{aligned}$$

where $\gamma_0 v = v|_{\Gamma}$ indicates the restriction of $v \in H^1(\Omega_i)$ on interface Γ , and $R_i : H_{00}^{\frac{1}{2}}(\Gamma) \rightarrow V_i$ any differentiable extension operator [38, 45]. Based on the minimum total potential energy

principle [10], we immediately obtain its equivalent variational form, that is,

$$\begin{aligned} & \arg \min_{u_1 \in V_1, u_1|_{\Gamma} = u_2} \frac{1}{2} a_1(u_1, u_1) - (f, u_1)_1, \\ & \arg \min_{u_2 \in V_2} \frac{1}{2} a_2(u_2, u_2) - (f, u_2)_2 - (f, R_1 \gamma_0 u_2)_1 + a_1(u_1, R_1 \gamma_0 u_2), \end{aligned}$$

and therefore the variational formulation of the iterative Dirichlet-Neumann algorithm [45, 38]: given the initial guess $h^{[0]} \in H_{00}^{\frac{1}{2}}(\Gamma)$, then solve for $k \geq 0$,

$$\begin{aligned} 1) \quad & u_1^{[k]} = \arg \min_{u_1 \in V_1, u_1|_{\Gamma} = h^{[k]}} \frac{1}{2} a_1(u_1, u_1) - (f, u_1)_1, \\ 2) \quad & u_2^{[k]} = \arg \min_{u_2 \in V_2} \frac{1}{2} a_2(u_2, u_2) - (f, u_2)_2 - (f, R_1 \gamma_0 u_2)_1 + a_1(u_1^{[k]}, R_1 \gamma_0 u_2), \\ 3) \quad & h^{[k+1]} = \rho u_2^{[k]} + (1 - \rho) h^{[k]} \quad \text{on } \Gamma, \end{aligned}$$

with $\rho \in (0, \rho_{\max})$ being the acceleration parameter [11]. Notably, the continuity of flux across the interface is guaranteed without explicitly calculating and exchanging local fluxes.

The variational formulation also makes it possible to integrate with the machine learning methods [47]. More precisely, the unknown solutions are parametrized by neural networks

$$(4.2) \quad u_1^{[k]}(x) \approx \hat{u}_1^{[k]}(x) := \hat{u}_1(x; \theta_1^{[k]}) \quad \text{and} \quad u_2^{[k]}(x) \approx \hat{u}_2^{[k]}(x) := \hat{u}_2(x; \theta_2^{[k]})$$

where $\hat{u}_i(x; \theta_i^{[k]})$ indicates the approximate solution with trained network parameters $\theta_i^{[k]}$ for $i = 1, 2$, and the network structure employed here could be a fully-connected neural network [12] or a residual neural network with several building blocks [15]. We note that in contrast to the finite element methods [45] where the extension is mesh-dependent and locally defined, the mesh-free neural network parametrization (4.2) can be regarded as a global function and thus provides a natural extension operator, *i.e.*, the neural network extension operator,

$$R_1 \gamma_0 \hat{u}_2(x, \theta_2) = \hat{u}_2(x, \theta_2)$$

which extends the restriction of $\hat{u}_2(x, \theta_2)$ on interface Γ to the subregion Ω_1 with zero boundary value on $\partial\Omega_1 \cap \partial\Omega$. Here, the requirement of homogeneous boundary condition is dealt with a soft manner by introducing the penalty function

$$\int_{\partial\Omega_1 \cap \partial\Omega} |\hat{u}_2|^2 ds$$

into the learning task (4.5) of the mixed Neumann-Dirichlet problem. Notably, as the extension operator is required to be differentiable, the hyperbolic tangent or sigmoid activation function should be used rather than the ReLU function.

Accordingly, by introducing the penalty term for enforcing essential boundary conditions,

the Dirichlet problem on Ω_1 can be formulated as*

$$(4.3) \quad \theta_1^{[k]} = \arg \min_{\theta_1} \int_{\Omega_1} \left(\frac{1}{2} |\nabla \hat{u}_1|^2 - f \hat{u}_1 \right) dx + \beta \left(\int_{\partial\Omega_1 \cap \partial\Omega} |\hat{u}_1|^2 ds + \int_{\Gamma} |\hat{u}_1 - h^{[k]}|^2 ds \right),$$

where $\beta > 0$ is a user-defined penalty coefficient. In fact, as the decomposition of equation leads to simpler functions to be learned on each subregion and hence the second-order derivatives can be explicitly involved during the training process, the residual form

$$(4.4) \quad \theta_1^{[k]} = \arg \min_{\theta_1} \int_{\Omega_1} |-\Delta \hat{u}_1 - f|^2 dx + \beta \left(\int_{\partial\Omega_1 \cap \partial\Omega} |\hat{u}_1|^2 ds + \int_{\Gamma} |\hat{u}_1 - h^{[k]}|^2 ds \right)$$

is preferred to the variational form (4.3) since the former is empirically found to be capable of offering more accurate estimates of the solution's gradient inside the computational domain [7]. On the other hand, the mixed Neumann-Dirichlet problem on Ω_2 can be written as

$$(4.5) \quad \theta_2^{[k]} = \arg \min_{\theta_2} \int_{\Omega_2} \left(\frac{1}{2} |\nabla \hat{u}_2|^2 - f \hat{u}_2 \right) dx + \int_{\Omega_1} \left(\nabla \hat{u}_1^{[k]} \cdot \nabla \hat{u}_2 - f \hat{u}_2 \right) dx + \beta \int_{\partial\Omega} |\hat{u}_2|^2 ds,$$

which relies on the gradient value $\nabla \hat{u}_1^{[k]}$ and therefore benefits from the residual form (4.4).

Now we are ready to discretize the functional integrals (4.3, 4.4) and (4.5), where the Monte Carlo method is adopted so as to overcome the curse of dimensionality [36]. Specifically, by generating the training sample points inside each subdomain and at its boundary, *i.e.*,

$$X_{\Omega_i} = \{x_n^{\Omega_i}\}_{n=1}^{N_{\Omega_i}}, \quad X_{D_i} = \{x_n^{D_i}\}_{n=1}^{N_{D_i}}, \quad \text{and} \quad X_{\Gamma} = \{x_n^{\Gamma}\}_{n=1}^{N_{\Gamma}},$$

where $D_i = \partial\Omega_i \cap \partial\Omega$, and the total number of points in the training datasets X_{Ω_i} , X_{D_i} , and X_{Γ} are denoted by N_{Ω_i} , N_{D_i} , and N_{Γ} , respectively. Consequently, by defining the following loss functions

$$L_{\Omega_i}(\hat{u}_i(x; \theta_i)) = \begin{cases} \frac{|\Omega_i|}{N_{\Omega_i}} \sum_{n=1}^{N_{\Omega_i}} |-\Delta \hat{u}_i(x_n^{\Omega_i}; \theta_i) - f(x_n^{\Omega_i})|^2 & \text{(residual form),} \\ \frac{|\Omega_i|}{N_{\Omega_i}} \sum_{n=1}^{N_{\Omega_i}} \left(\frac{1}{2} |\nabla \hat{u}_i(x_n^{\Omega_i}; \theta_i)|^2 - f(x_n^{\Omega_i}) \hat{u}_i(x_n^{\Omega_i}; \theta_i) \right) & \text{(variational form),} \end{cases}$$

$$L_{D_i}(\hat{u}_j(x; \theta_j)) = \frac{|\partial\Omega_i \setminus \Gamma|}{N_{D_i}} \sum_{n=1}^{N_{D_i}} |\hat{u}_j(x_n^{D_i}; \theta_j)|^2, \quad L_{\Gamma}(\hat{u}_1(x; \theta_1)) = \frac{|\Gamma|}{N_{\Gamma}} \sum_{n=1}^{N_{\Gamma}} |\hat{u}_1(x_n^{\Gamma}; \theta_1) - h^{[k]}(x_n^{\Gamma})|^2,$$

$$L_N(\hat{u}_2(x; \theta_2), \hat{u}_1(x; \theta_1^{[k]})) = \frac{|\Omega_1|}{N_{\Omega_1}} \sum_{n=1}^{N_{\Omega_1}} \left(\nabla \hat{u}_1(x_n^{\Omega_1}; \theta_1^{[k]}) \cdot \nabla \hat{u}_2(x_n^{\Omega_1}; \theta_2) - f(x_n^{\Omega_1}) \hat{u}_2(x_n^{\Omega_1}; \theta_2) \right),$$

the learning task associated with (4.3, 4.4) is defined as

$$(4.6) \quad \theta_1^{[k]} = \arg \min_{\theta_1} L_{\Omega_1}(\hat{u}_1(x; \theta_1)) + \beta \left(L_{D_1}(\hat{u}_1(x; \theta_1)) + L_{\Gamma}(\hat{u}_1(x; \theta_1)) \right),$$

*For notational simplicity, $\hat{u}_1(x, \theta_1)$ and $\hat{u}_2(x, \theta_2)$ are abbreviated as \hat{u}_1 and \hat{u}_2 if not specified otherwise.

while that of the functional integral (4.5) is given by

$$(4.7) \quad \theta_2^{[k]} = \arg \min_{\theta_2} L_{\Omega_2}(\hat{u}_2(x; \theta_2)) + L_N(\hat{u}_2(x; \theta_2), \hat{u}_1(x; \theta_1^{[k]})) + \beta \left(L_{D_1}(\hat{u}_2(x; \theta_2)) + L_{D_2}(\hat{u}_2(x; \theta_2)) \right).$$

Clearly, even though the network solution of the Dirichlet subproblem on Ω_1 is prone to overfitting on the interface [9, 1], it can be observed from (4.7) that the mixed Neumann-Dirichlet problem on Ω_2 can be solved without explicitly computing and enforcing the flux transmission condition across subdomain interfaces. Moreover, as the second-order derivatives are explicitly involved during the training process of Dirichlet subproblems (4.4), the network approximation to the solution's gradient is rather accurate inside each subregion, which is highly desirable for solving the mixed Neumann-Dirichlet problem (4.5).

To sum up, by using our compensated deep Ritz method, the proposed Dirichlet-Neumann learning algorithm is presented in algorithm 4.1, where the mini-batch data computed during training are not relabelled for notational simplicity, and the stopping criteria can be constructed by measuring the difference between two consecutive iterations [29]. We also note that, though the Dirichlet-Neumann learning algorithm 4.1 has sequential steps that inherited from the original Dirichlet-Neumann approach [45, 38], various techniques have been developed to solve subproblems in parallel (see [33] and references cited therein), which is left for future investigation.

Remark 4.1. Our compensated deep Ritz method (or the Dirichlet-Neumann learning algorithm 4.1) can also be easily extended to solve the more challenging elliptic interface problem with high-contrast coefficients [31, 14]

$$\begin{aligned} -\nabla \cdot (c(x) \nabla u(x)) &= f(x) & \text{in } \Omega, \\ u(x) &= 0 & \text{on } \partial\Omega, \end{aligned}$$

where $\Gamma = \partial\Omega_1 \cap \partial\Omega_2$ is an immersed interface (see Figure 2), the coefficient function $c(x)$ is piecewise constant with respect to the decomposition of domain

$$c(x) = \begin{cases} c_1 > 0 & \text{in } \Omega_1, \\ c_2 > 0 & \text{in } \Omega_2, \end{cases}$$

and the natural jump conditions [31] are defined as

$$[u] = 0 \quad \text{and} \quad \left[c \frac{\partial u}{\partial \mathbf{n}} \right] = q \quad \text{on } \Gamma.$$

Applying Green's formula in each subdomain and adding them together, we obtain the weak formulation for the high-contrast problem, *i.e.*, find $u_1 \in V_1$ and $u_2 \in V_2$ such that

$$\begin{aligned} b_1(u_1, v_1) &= (f, v_1)_1 & \text{for any } v_1 \in V_1^0, \\ u_1 &= u_2 & \text{on } \Gamma, \\ b_2(u_2, v_2) &= (f, v_2)_2 + (f, R_1 \gamma_0 v_2)_1 - b_1(u_1, R_1 \gamma_0 v_2) - (q, v_2)_\Gamma, & \text{for any } v_2 \in V_2, \end{aligned}$$

Algorithm 4.1 Dirichlet-Neumann Learning Algorithm for Two Subdomains

```

% Initialization
– divide domain  $\Omega \subset \mathbb{R}^d$  into two non-overlapping subregions  $\Omega_1$  and  $\Omega_2$ ;
– specify network structures  $\hat{u}_1(x; \theta_1)$  and  $\hat{u}_2(x; \theta_2)$  for each subproblem;
– generate Monte Carlo training samples  $X_\Gamma$ ,  $X_{\Omega_i}$ , and  $X_{D_i}$  for  $i = 1, 2$ ;
% Outer Iteration Loop
Start with the initial guess  $h^{[0]}$  along the interface  $\Gamma$ ;
for  $k \leftarrow 0$  to  $K$  (maximum number of outer iterations) do
  while stopping criteria are not satisfied do
    % Dirichlet Subproblem-Solving via Solution-Oriented Learning Method
    for  $\ell \leftarrow 0$  to  $L$  (maximum number of training epochs) do
      for  $m \leftarrow 0$  to  $M$  (maximum number of training mini-batches) do
        – draw mini-batch data uniformly at random from  $X_\Gamma$ ,  $X_{\Omega_1}$ , and  $X_{D_1}$ ;
        – network training by employing the physics-informed neural network (4.6), i.e.,
          
$$\theta_1^{[k]} = \arg \min_{\theta_1} L_{\Omega_1}(\hat{u}_1) + \beta \left( L_{D_1}(\hat{u}_1) + L_\Gamma(\hat{u}_1) \right)$$

      end for
    end for
    % Neumann Subproblem-Solving via Compensated Deep Ritz Method
    for  $\ell \leftarrow 0$  to  $L$  (maximum number of training epochs) do
      for  $m \leftarrow 0$  to  $M$  (maximum number of training mini-batches) do
        – draw mini-batch data uniformly at random from  $X_{\Omega_1}$ ,  $X_{\Omega_2}$ ,  $X_{D_1}$ , and  $X_{D_2}$ ;
        – network training by employing the compensated deep Ritz method (4.7), i.e.,
          
$$\theta_2^{[k]} = \arg \min_{\theta_2} L_{\Omega_2}(\hat{u}_2) + L_N(\hat{u}_2, \hat{u}_1^{[k]}) + \beta \left( L_{D_1}(\hat{u}_2) + L_{D_2}(\hat{u}_2) \right)$$

      end for
    end for
    % Update of boundary values at interface  $\Gamma$  for Dirichlet subproblem
    for  $n \leftarrow 1$  to  $N_\Gamma$  do
      
$$h^{[k+1]}(x_n^\Gamma) = \rho \hat{u}_2(x_n^\Gamma; \theta_2^{[k]}) + (1 - \rho) h^{[k]}(x_n^\Gamma)$$

    end for
  end while
end for

```

where the bilinear forms are defined as

$$b_i(u_i, v_i) = \int_{\Omega_i} c_i \nabla u_i \cdot \nabla v_i \, dx, \quad (f, v_i)_i = \int_{\Omega_i} f v_i \, dx, \quad \text{and} \quad (q, v_2)_\Gamma = \int_\Gamma q v \, ds,$$

for $i = 1, 2$. By resorting to the variational form [10, 5] and parametrizing the trial functions as neural networks, i.e., $u_i(x) \approx \hat{u}_i(x; \theta_i)$ for $i = 1, 2$, the learning task associated with the

Dirichlet problem[†] on Ω_1 gives

$$(4.8) \quad \theta_1^{[k]} = \arg \min_{\theta_1} \int_{\Omega_1} |-\nabla \cdot (c_1 \nabla \hat{u}_1) - f|^2 dx + \beta \left(\int_{\partial\Omega_1 \cap \partial\Omega} |\hat{u}_1|^2 ds + \int_{\Gamma} |\hat{u}_1 - \hat{u}_2|^2 ds \right),$$

and that of the mixed Neumann-Dirichlet problem on Ω_2 takes on the form

$$(4.9) \quad \theta_2^{[k]} = \arg \min_{\theta_2} \int_{\Omega_2} \left(\frac{c_2}{2} |\nabla \hat{u}_2|^2 - f \hat{u}_2 \right) dx + \int_{\Omega_1} \left(c_1 \nabla \hat{u}_1^{[k]} \cdot \nabla \hat{u}_2 - f \hat{u}_2 \right) dx + \int_{\Gamma} q \hat{u}_2 ds + \beta \int_{\partial\Omega} |\hat{u}_2|^2 ds.$$

Therefore, an iterative learning approach for solving the elliptic interface problem with high-contrast coefficients can be immediately constructed from (4.8) and (4.9).

4.2. Neumann-Neumann Learning Algorithm. Similar in spirit, the compensated deep Ritz method can be applied to construct the Neumann-Neumann learning algorithm (see Figure 1). Using the same notations as before, the iterative Neumann-Neumann scheme (see Algorithm 2.2) can be written in an equivalent variational form: given the initial guess $h^{[0]} \in H_{00}^{\frac{1}{2}}(\Gamma)$, then solve for $k \geq 0$ and $i = 1, 2$,

- 1) $u_i^{[k]} = \arg \min_{u_i \in V_i, u_i|_{\Gamma} = h^{[k]}} \frac{1}{2} a_i(u_i, u_i) - (f, u_i)_i,$
- 2) $\psi_i^{[k]} = \arg \min_{\psi_i \in V_i} \frac{1}{2} a_i(\psi_i, \psi_i) + (f, \psi_i)_i + (f, R_{3-i} \gamma_0 \psi_i)_{3-i} - a_i(u_i^{[k]}, \psi_i) - a_{3-i}(u_{3-i}^{[k]}, R_{3-i} \gamma_0 \psi_i),$
- 3) $h^{[k+1]} = h^{[k]} - \rho(\psi_1^{[k]} + \psi_2^{[k]}) \quad \text{on } \Gamma,$

with $\rho \in (0, \rho_{\max})$ being the acceleration parameter. Next, by parametrizing the trial functions as neural networks, that is,

$$u_i^{[k]}(x) \approx \hat{u}_i^{[k]}(x) := \hat{u}_i(x; \theta_i^{[k]}) \quad \text{and} \quad \psi_i^{[k]}(x) \approx \hat{\psi}_i^{[k]}(x) := \hat{\psi}_i(x; \eta_i^{[k]})$$

for $i = 1, 2$, and by employing the neural network extension operators

$$R_1 \gamma_0 \hat{\psi}_2(x, \eta_2) = \hat{\psi}_2(x, \eta_2) \quad \text{and} \quad R_2 \gamma_0 \hat{\psi}_1(x, \eta_1) = \hat{\psi}_1(x, \eta_1),$$

the learning tasks associated with the Neumann-Neumann algorithm can be formulated as

$$\theta_i^{[k]} = \arg \min_{\theta_i} \int_{\Omega_i} |-\Delta \hat{u}_i - f|^2 dx + \beta \left(\int_{\partial\Omega_i \cap \partial\Omega} |\hat{u}_i|^2 ds + \int_{\Gamma} |\hat{u}_i - h^{[k]}|^2 ds \right),$$

$$\eta_i^{[k]} = \arg \min_{\eta_i} \int_{\Omega_i} \left(\frac{1}{2} |\nabla \hat{\psi}_i|^2 + f \hat{\psi}_i - \nabla \hat{u}_i^{[k]} \cdot \nabla \hat{\psi}_i \right) dx + \int_{\Omega_{3-i}} \left(f \hat{\psi}_i - \nabla \hat{u}_{3-i}^{[k]} \cdot \nabla \hat{\psi}_i \right) dx + \beta \int_{\partial\Omega} |\hat{\psi}_i|^2 ds,$$

where $\beta > 0$ is a user-defined penalty coefficient, $i = 1, 2$, and the training tasks associated with Dirichlet subproblems are defined in a residual form as before. Therefore, the iterative learning approach can be constructed by using numerical integration formulas.

[†]Here, the residual form is used instead since the solution on each subregion is rather smooth, resulting in more accurate approximation of the solution's gradient inside the subdomain.

4.3. Dirichlet-Dirichlet Learning Algorithm. To build the Dirichlet-Dirichlet learning algorithm in Figure 1, we first rewrite the iterative process (see Algorithm 2.2) as: given the initial guess $h^{[0]} \in H_{00}^{\frac{1}{2}}(\Gamma)$ and $\psi_1^{[0]} = \psi_2^{[0]} = 0$, then solve for $k \geq 0$,

$$\begin{aligned} 1) \text{ solve on } \Omega_i \text{ for } u_i^{[k]}: & \begin{cases} -\Delta u_i^{[k]} = f & \text{in } \Omega_i, \\ u_i^{[k]} = 0 & \text{on } \partial\Omega \cap \partial\Omega_i, \\ \nabla u_i^{[k]} \cdot \mathbf{n}_i = h^{[k]} - \theta(\nabla \psi_1^{[k]} \cdot \mathbf{n}_1 + \nabla \psi_2^{[k]} \cdot \mathbf{n}_2) & \text{on } \Gamma, \end{cases} \\ 2) \text{ solve on } \Omega_i \text{ for } \psi_i^{[k+1]}: & \begin{cases} -\Delta \psi_i^{[k+1]} = 0 & \text{in } \Omega_i, \\ \psi_i^{[k+1]} = 0 & \text{on } \partial\Omega \cap \partial\Omega_i, \\ \psi_i^{[k+1]} = u_1^{[k]} - u_2^{[k]} & \text{on } \Gamma, \end{cases} \end{aligned}$$

where $i = 1, 2$. Using the same notations as before, the Green's theorem indicates that the the variational formulation of the mixed Neumann-Dirichlet problem reads: for $i = 1, 2$,

$$u_i^{[k]} = \arg \min_{u_i \in V_i} \frac{1}{2} a_i(u_i, u_i) - (f, u_i)_i - (h^{[k]}, u_i)_\Gamma + \rho(a_i(\psi_i^{[k]}, u_i) + a_{3-i}(\psi_{3-i}^{[k]}, R_{3-i}\gamma_0 u_i))$$

where $(\cdot, \cdot)_\Gamma$ denotes the L_2 inner product on Γ , $\rho \in (0, \rho_{\max})$, and the Dirichlet problem is reformulated as

$$\psi_i^{[k]} = \arg \min_{\psi_i \in V_i, \psi_i|_\Gamma = u_1^{[k]} - u_2^{[k]}} \frac{1}{2} a_i(\psi_i, \psi_i)$$

for $i = 1, 2$. Consequently, by parametrizing the trial functions as neural networks, *i.e.*,

$$u_i^{[k]}(x) \approx \hat{u}_i^{[k]}(x) := \hat{u}_i(x; \theta_i^{[k]}) \quad \text{and} \quad \psi_i^{[k]}(x) \approx \hat{\psi}_i^{[k]}(x) := \hat{\psi}_i(x; \eta_i^{[k]})$$

for $i = 1, 2$, and by employing the neural network extension operators

$$R_1\gamma_0\hat{u}_2(x, \theta_2) = \hat{u}_2(x, \theta_2) \quad \text{and} \quad R_2\gamma_0\hat{u}_1(x, \theta_1) = \hat{u}_1(x, \theta_1),$$

the learning tasks associated with the Dirichlet-Dirichlet algorithm can be formulated as

$$\begin{aligned} \theta_i^{[k]} &= \arg \min_{\theta_i} \int_{\Omega_i} \left(\frac{1}{2} |\nabla \hat{u}_i|^2 - f \hat{u}_i + \rho \nabla \hat{\psi}_i^{[k]} \cdot \nabla \hat{u}_i \right) dx + \rho \int_{\Omega_{3-i}} \nabla \hat{\psi}_{3-i}^{[k]} \cdot \nabla \hat{u}_i dx \\ &\quad - \int_\Gamma h^{[k]} \hat{u}_i ds + \beta \int_{\partial\Omega_i \cap \partial\Omega} |\hat{u}_i|^2 ds, \\ \eta_i^{[k]} &= \arg \min_{\eta_i} \int_{\Omega_i} |\Delta \hat{\psi}_i|^2 dx + \beta \left(\int_{\partial\Omega_i \cap \partial\Omega} |\hat{\psi}_i|^2 ds + \int_\Gamma |\hat{\psi}_i - \hat{u}_1^{[k]} + \hat{u}_2^{[k]}|^2 ds \right), \end{aligned}$$

where $\beta > 0$ is a user-defined penalty coefficient, $i = 1, 2$, and the training tasks associated with Dirichlet subproblems are defined in a residual form as before.

4.4. Robin-Robin Learning Algorithm. As mentioned before, the Robin-Robin algorithm only requires solution exchange between neighbouring subdomains, however, it may still suffer from the problem of overfitted interface conditions. More specifically, let $\kappa_1 = 1$ in what follows, then a relatively large value of $\kappa_2 > 0$ is typically required in order to reduce the total number of outer iterations [8]. When the Robin boundary condition is incorporated as the soft penalty term during training, it may cause weights imbalance between the solution and its gradient on the interface, thereby making the trained model prone to overfitting at and near the interfaces. To alleviate the issue of weights imbalance, the compensated deep Ritz method is a promising alternative for realizing the deep learning analogue of the classical Robin-Robin algorithm.

Note that in terms of differential operator, the second subproblem with $\kappa_2 \gg \kappa_1 = 1$ in the Robin-Robin algorithm [38] can be rewritten as

$$\begin{cases} -\Delta u_2^{[k]} = f & \text{in } \Omega_2, \\ u_2^{[k]} = 0 & \text{on } \partial\Omega \cap \partial\Omega_2, \\ \kappa_2 u_2^{[k]} + \nabla u_2^{[k]} \cdot \mathbf{n}_2 = \kappa_2 u_1^{[k]} - \nabla u_1^{[k]} \cdot \mathbf{n}_1 & \text{on } \Gamma. \end{cases}$$

Using the same notations as before, it is equivalent to find the weak solution $u_2^{[k]} \in V_2$ such that

$$(4.10) \quad a_2(u_2^{[k]}, v_2) = (f, v_2)_2 + (\kappa_2(u_1^{[k]} - u_2^{[k]} - \nabla u_1^{[k]} \cdot \mathbf{n}_1), v_2)_\Gamma \quad \text{for any } v_2 \in V_2.$$

Next, by using the Green's formula, we arrive at another form of (4.10), that is,

$$a_2(u_2^{[k]}, v_2) = (f, v_2)_2 + \kappa_2(u_1^{[k]} - u_2^{[k]}, v_2)_\Gamma - a_1(u_1^{[k]}, R_1\gamma_0 v_2) + (f, R_1\gamma_0 v_2)_1 \quad \text{for any } v_2 \in V_2$$

and therefore the variational formulation of (4.10) due to the symmetry of bilinear forms

$$u_2^{[k]} = \arg \min_{u_2 \in V_2} \frac{1}{2} a_2(u_2, u_2) - (f, u_2)_2 - \kappa_2(u_1^{[k]} - \frac{1}{2} u_2, u_2)_\Gamma + a_1(u_1^{[k]}, R_1\gamma_0 u_2) - (f, R_1\gamma_0 u_2)_1$$

which completely differs from the original PINN approach (3.1).

As such, by parametrizing the trial functions as neural networks, *i.e.*,

$$u_1^{[k]}(x) \approx \hat{u}_1^{[k]}(x) := \hat{u}_1(x, \theta_1^{[k]}) \quad \text{and} \quad u_2^{[k]}(x) \approx \hat{u}_2^{[k]}(x) := \hat{u}_2(x, \theta_2^{[k]}),$$

and by employing the neural network extension operator

$$R_1\gamma_0 \hat{u}_2(x, \theta_2) = \hat{u}_2(x, \theta_2),$$

the learning task associated with the second Robin problem takes on the form:

$$\begin{aligned} \theta_2^{[k]} = \arg \min_{\theta_2} \int_{\Omega_2} \left(\frac{1}{2} |\nabla \hat{u}_2|^2 - f \hat{u}_2 \right) dx - \kappa_2 \int_{\Gamma} \left(\hat{u}_1^{[k]} \hat{u}_2 - \frac{1}{2} |\hat{u}_2|^2 \right) ds \\ + \int_{\Omega_1} \left(\nabla \hat{u}_1^{[k]} \cdot \nabla \hat{u}_2 - f \hat{u}_2 \right) dx + \beta \int_{\partial\Omega} |\hat{u}_2|^2 ds, \end{aligned}$$

which obviously removes the issue of weights imbalance between the solution value and its normal derivatives on the interface.

5. Numerical Experiments. To validate the effectiveness of our proposed domain decomposition learning algorithms, we conduct experiments using the Dirichlet-Neumann and Robin-Robin learning algorithms on a wide range of elliptic boundary value problems in this section, while the Neumann-Neumann and Dirichlet-Dirichlet learning algorithms are omitted due to the limitation of pages. In what follows, our proposed Dirichlet-Neumann learning method, *i.e.*, algorithm 4.1, is abbreviated as DNLM for simplicity, with bracket indicating the numerical solver adopted for solving the Dirichlet subproblems. In contrast to our proposed methods, the existing learning approach [30] for realizing the classical Dirichlet-Neumann algorithm is based on a direct substitution of the numerical solvers with the PINN approach, which is referred to as DN-PINNs and is used for comparison. On the other hand, although the update of interface conditions in the Robin-Robin algorithm does not directly depends on the flux exchange, it may still suffer from the weights imbalance and therefore the interface overfitting. To further investigate the overfitting effects, the Robin-Robin algorithm is realized using the standard PINN approach and our compensated deep Ritz method after the empirical study of DNLM, which is referred to as RR-PINNs, RRLM (PINN), and RRLM (deep Ritz) in a similar fashion.

As is common for practical implementation [30, 23], the network architecture deployed for each subregion is a fully connected network with 3 hidden layers of 50 neurons each [12], while the hyperbolic tangent activation function is employed due to the smoothness of local solutions and the differentiability of extension operators. During the training mode and for $i = 1, 2$, we randomly sample $N_{\Omega_i} = 20000$ points from the interior domain Ω_i , $N_\Gamma = 5000$ points from the interface Γ , and $N_D = 5000$ points from the boundary $\partial\Omega_i \setminus \Gamma$ of length Γ each. Then the trained models are evaluated the test dataset, *i.e.*, $N_\Omega = 10000$ points that are uniformly distributed over the entire computational domain, and compared with the true solution to test their performance. The penalty coefficient is set to be $\beta = 400$ and the number of mini-batches is chosen as 5 for all training datasets. When executing the learning task on each subdomain, the initial learning rate of Adam optimizer is set to be 0.1, which is divided by 10 at the 600 and 800 epochs. The training process is terminated after 1000 epochs for each decomposed subproblem, and the model with minimum training loss is chosen to execute the subsequent operations. All the experiments are implemented using PyTorch and trained on the NVIDIA GeForce RTX 2060.

5.1. Dirichlet-Neumann Learning Algorithm. As a representative benchmark, we consider the learning approaches for realizing the classical Dirichlet-Neumann algorithm. More precisely, a comparison study between DN-PINNs, DNLM (PINN), and DNLM (deep Ritz) is presented in this subsection, where experiments on a wide variety of elliptic problems are conducted to demonstrate the effectiveness and flexibility of our proposed methods.

5.1.1. Poisson's Equation with Simple Interface. To begin with, we consider a benchmark Poisson problem in the two-dimensional case, that is,

$$(5.1) \quad \begin{aligned} -\Delta u(x, y) &= 4\pi^2 \sin(2\pi x)(2 \cos(2\pi y) - 1) & \text{in } \Omega = (0, 1)^2, \\ u(x, y) &= 0 & \text{on } \partial\Omega, \end{aligned}$$

where the exact solution is given by $u(x, y) = \sin(2\pi x)(\cos(2\pi y) - 1)$, and the interface $\Gamma = \partial\Omega_1 \cap \partial\Omega_2$ is a straight line segment from $(0.5, 0)$ to $(0.5, 1)$ as depicted in Figure 3. It is noteworthy that although the exact solution on each subregion is rather smooth, its normal derivative on the interface is non-trivial that may bring difficulties for network training [1], this differs from the widely-used non-overlapping example that has trivial gradients on the interface [30].

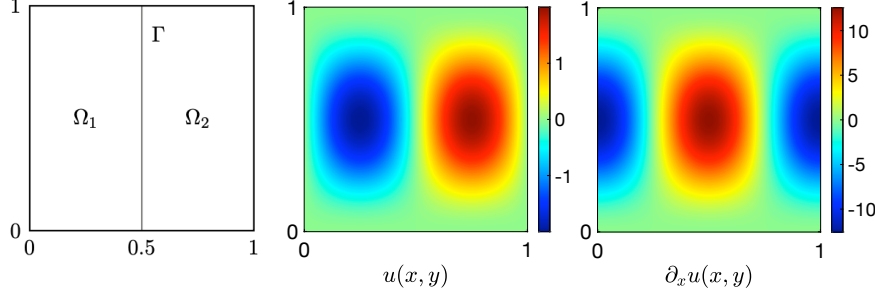


Figure 3: From left to right: decomposition of domain into two subregions, exact solution $u(x, y)$, and its partial derivatives $\partial_x u(x, y)$ for the numerical example (5.1).

Based on the conventional Dirichlet-Neumann algorithm [45, 38] that is defined in terms of differential operators, we first conduct experiments using the most commonly used PINNs [39, 23] as the numerical solver of all decomposed subproblems. We show in Figure 4a the iterative numerical solutions over the entire computational domain in a typical simulation, and in Figure 4b the corresponding pointwise absolute errors. Here, the initial guess for the Dirichlet interface condition is set to be

$$h^{[0]}(x, y) = \sin(2\pi x)(\cos(2\pi y) - 1) - 50xy(x - 1)(y - 1) \quad \text{on } \Gamma,$$

which remains unchanged for the methods tested below. Unfortunately, DN-PINNs fails to converge to the correct solution of (5.1) shown in Figure 4, since the trained networks are prone to overfitting on the interface [9]. In other words, with the interface conditions being included as extra soft constraints in the loss function and the size of training data on interface being smaller than that of interior domains, the trained model using standard PINN approach [39] suffers from the issue of boundary overfitting [9, 1], and therefore fails to be accurate enough for the prediction of local fluxes even if the training loss is very small. As a result, it would hamper the convergence of outer iteration but is perhaps inevitable in practice for problems with complex interface conditions. In fact, a straightforward replacement of the numerical solvers by other learning strategies, *e.g.*, the deep Ritz method [47], also has the same issue.

In contrast, although the predicted flux through the network solution of Dirichlet subproblem is usually of unacceptable low accuracy, our proposed method doesn't need to explicitly enforce the flux continuity condition along the interface, thereby enabling the effectiveness of outer iteration in the presence of overfitted interface (see Figure 7). To validate our statements, we show in Figure 5 and Figure 6 the computational results using our Dirichlet-Neumann learning algorithm 4.1, where the PINN [39] and the deep Ritz method [47] are employed for

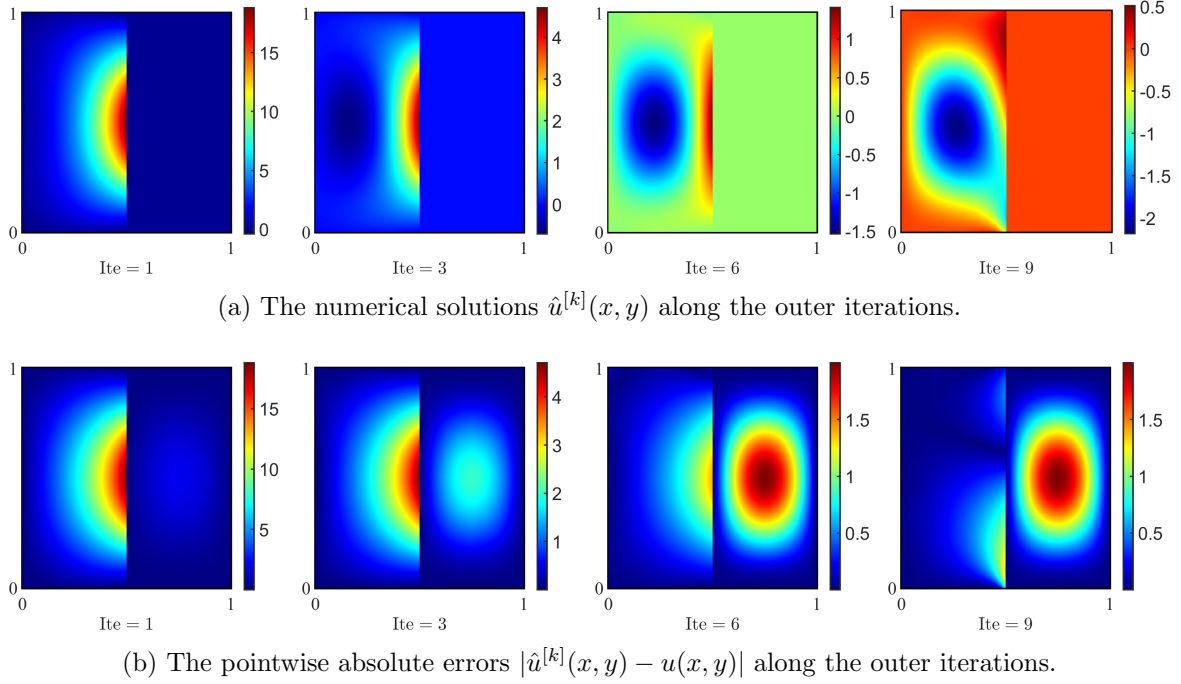


Figure 4: Numerical results of example (5.1) using the DN-PINNs on the test dataset.

solving the Dirichlet subproblem, respectively.

As can be observed from Figure 5 and Figure 6, the predicted solution using our learning methods is in agreement with the true solution over the entire computational domain, while the corresponding first-order derivatives shown in Figure 7 indicate that the network solution of Dirichlet subproblem rather learns to overfit at the interface. More quantitatively, we run the simulations for 5 times to calculate the relative L_2 errors, and the results (mean value \pm standard deviation) are reported in Table 1 and Figure 8. By employing our proposed compensated deep Ritz method for solving the mixed Neumann-Dirichlet subproblem, it is obvious that our learning algorithms converge to the exact solution very well, while the DN-PINNs is typically divergent due to the lack of accurate flux estimation along the interface. Moreover, as the solution of (5.1) is rather smooth on each subregion, it can be found in Table 1 and Figure 8 that the DNLM (PINN) performs better than the DNLM (deep Ritz). This is because that the second-order derivatives are explicitly involved during training, leading to better estimates of the solution's gradient inside the computational domain (see Figure 7).

5.1.2. Poisson's Equation with Zigzag Interface. To demonstrate the advantage of our mesh-free approach over the traditional mesh-based numerical methods [45], we consider the previous example but with a more complex interface geometry, namely,

$$(5.2) \quad \begin{aligned} -\Delta u(x, y) &= 4\pi^2 \sin(2\pi y)(2 \cos(2\pi x) - 1) & \text{in } \Omega = (0, 1)^2, \\ u(x, y) &= 0 & \text{on } \partial\Omega, \end{aligned}$$

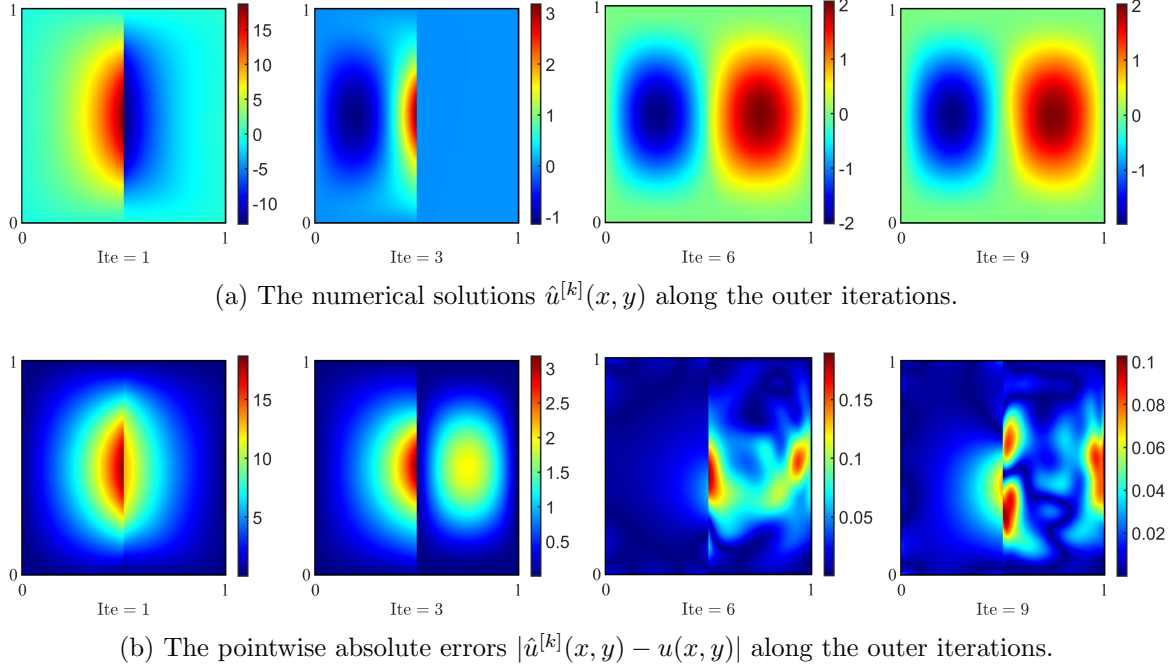


Figure 5: Numerical results of example (5.1) using our DNLM (PINN) on the test dataset.

Table 1: Relative L_2 errors of the predicted solution along the outer iteration k for example (5.1), with mean value (\pm standard deviation) being reported over 5 runs.

Outer Iterations		1	3	5	7	9
Relative Errors						
$\frac{\ \hat{u}^{[k]} - u\ _{L_2(\Omega)}}{\ u\ _{L_2(\Omega)}}$	DN-PINNs	24.16 (± 48.04)	6.70 (± 12.10)	2.28 (± 2.70)	0.91 (± 0.52)	1.15 (± 0.49)
	DNLM (PINN)	9.16 (± 2.34)	2.81 (± 0.56)	1.17 (± 0.71)	0.08 (± 0.07)	0.10 (± 0.04)
	DNLM (Deep Ritz)	9.50 (± 2.46)	1.83 (± 0.86)	0.41 (± 0.35)	0.62 (± 0.55)	0.40 (± 0.49)

where the exact solution is defined as $u(x, y) = \sin(2\pi y)(\cos(2\pi x) - 1)$ and the interface is a curved zigzag line as depicted in Figure 9. More precisely, the zigzag function reads

$$x = c(a(20y - \text{floor}(20y)) + b) + 0.5$$

where coefficients $a = 0.05(-1 + 2 \times \text{mod}(\text{floor}(20y), 2))$, $b = -0.05 \times \text{mod}(\text{floor}(20x), 2)$ and $c = -2 \times \text{mod}(\text{floor}(10x), 2) + 1$, thereby enabling the sample generation process inside each subdomain and along its boundaries. Our proposed learning algorithm 4.1 can easily handle

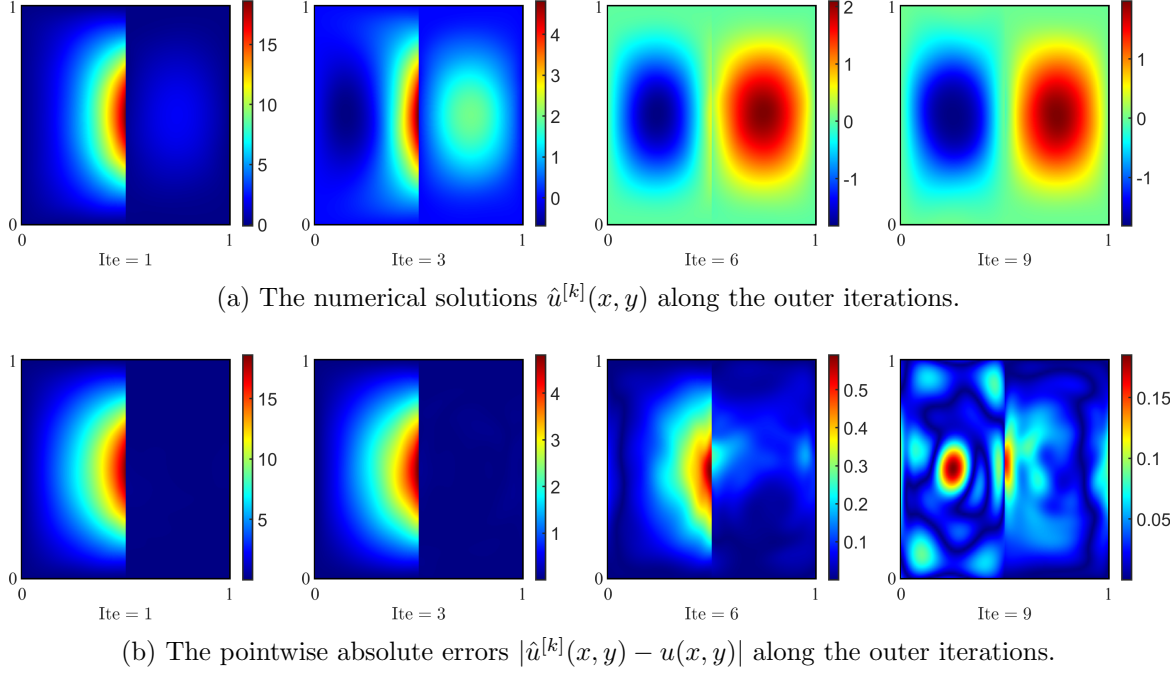


Figure 6: Numerical results of example (5.1) using our DNLM (deep Ritz) on the test dataset.

such irregular boundary shapes (see Figure 11 and Figure 12), while the traditional finite difference or finite element method [5] calls for a computationally expensive mesh generation procedure.

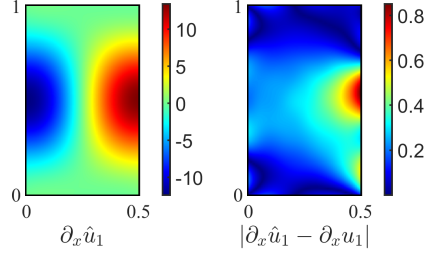
We first conduct experiments using the DN-PINNs scheme [29] for solving (5.2), and the numerical results in a typical simulation are depicted in Figure 10. Here, the initial guess is

$$h^{[0]}(x, y) = \sin(2\pi x)(\cos(2\pi y) - 1) - 1000 \sin(2\pi x)^2 \sin(2\pi y) \quad \text{on } \Gamma,$$

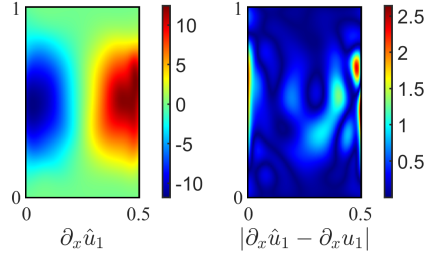
which remains unchanged for other methods tested below. Similar as before, the DN-PINNs scheme fails to converge to the exact solution shown in Figure 9, since the network solution of Dirichlet subproblem learns to satisfy the constrained equations but for an overfitted interface condition.

On the other hand, by replacing the numerical solver of Neumann subproblem with our compensated deep Ritz method, the numerical results depicted in Figure 11[‡] indicate that our DNLM (PINN) approach can obtain a satisfactory approximation to the exact solution of (5.2), which circumvents the meshing procedure that remains challenging for problems with complex interfaces. Moreover, our learning approaches remain effective in the presence of interface overfitting (see Figure 13), and therefore is highly desirable in practice since overfitting always occurs to a greater or lesser extent.

[‡]The first figure in Figure 11a means that the current solution is still far away from the real one, which is



(a) Network solution $\partial_x \hat{u}_1^{[9]}(x, y)$ and its error $|\partial_x \hat{u}_1^{[9]}(x, y) - \partial_x u_1(x, y)|$ using DNLM (PINN).



(b) Network solution $\partial_x \hat{u}_1^{[9]}(x, y)$ and its error $|\partial_x \hat{u}_1^{[9]}(x, y) - \partial_x u_1(x, y)|$ using DNLM (deep Ritz).

Figure 7: Overfitting phenomenon in solving the Dirichlet subproblem of (5.1) on testdata.

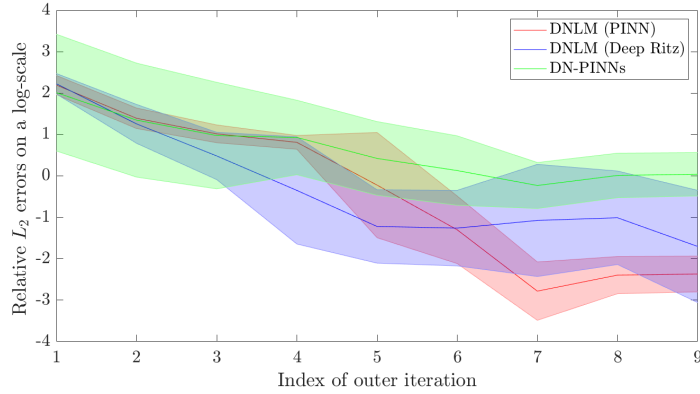


Figure 8: Relative L_2 errors on testdata along outer iterations for example (5.1).

Note that when the deep Ritz method [47] is adopted for solving the Dirichlet subproblem, the accuracy of approximate gradients inside the computational domain is no longer comparable to that of PINN approach [7]. The situation is susceptible to become even worse for irregular domains, and therefore the DNLM (deep Ritz) may fail to be accurate enough as

not restated in what follows.

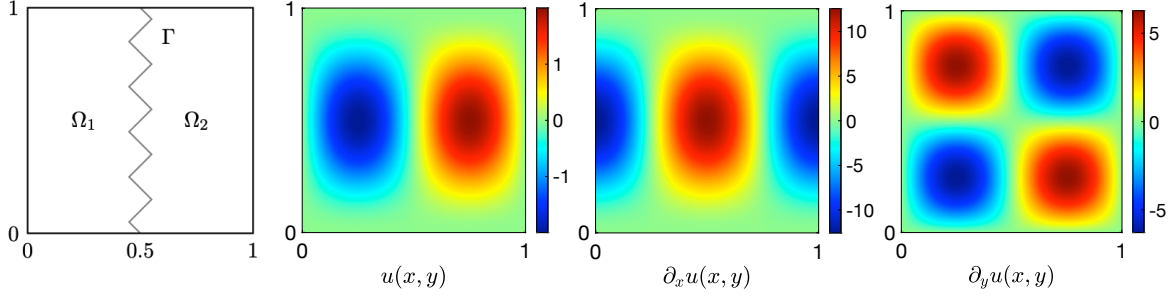
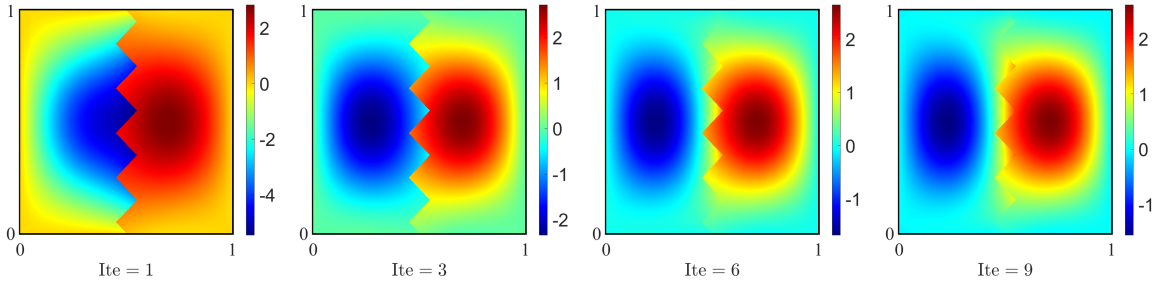
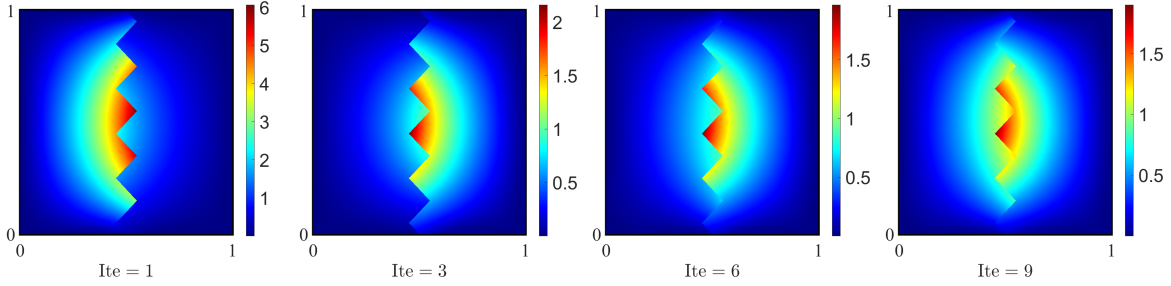


Figure 9: From left to right: decomposition of domain into two subregions, exact solution $u(x, y)$, and its partial derivatives $\partial_x u(x, y)$, $\partial_y u(x, y)$ for the numerical example (5.2).



(a) The numerical solutions $\hat{u}^{[k]}(x, y)$ along the outer iterations.



(b) The pointwise absolute errors $|\hat{u}^{[k]}(x, y) - u(x, y)|$ along the outer iterations.

Figure 10: Numerical results of example (5.1) using the DN-PINNs on the test dataset.

shown in Figure 12. To further validate our statements, we show in Table 2 and Figure 14 the quantitative results over 5 runs, where DNLM (PINN) outperforms DN-PINNs and DNLM (deep Ritz) in terms of accuracy.

5.1.3. Poisson's Equation with Four Subdomains. Next, we consider the Poisson problem divided into four subproblems in two-dimension, that is,

$$(5.3) \quad \begin{aligned} -\Delta u(x, y) &= f(x, y) & \text{in } \Omega = (0, 1)^2, \\ u(x, y) &= 0 & \text{on } \partial\Omega, \end{aligned}$$

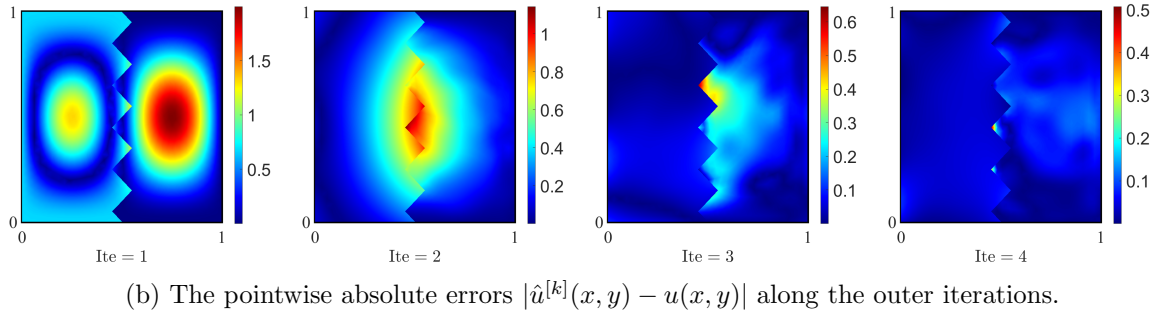
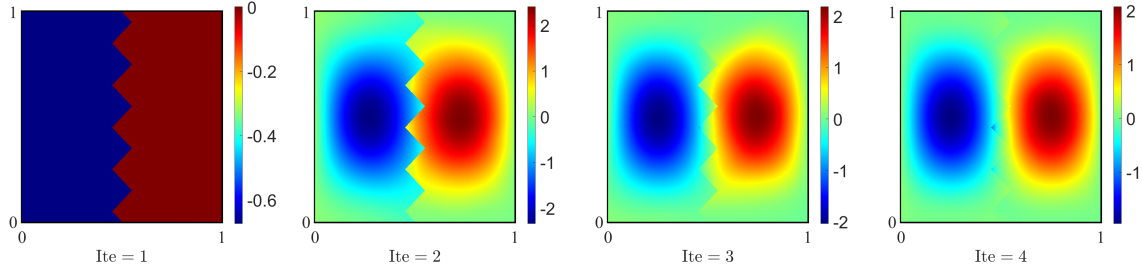


Figure 11: Numerical results of example (5.2) using our DNLM (PINN) on the test dataset.

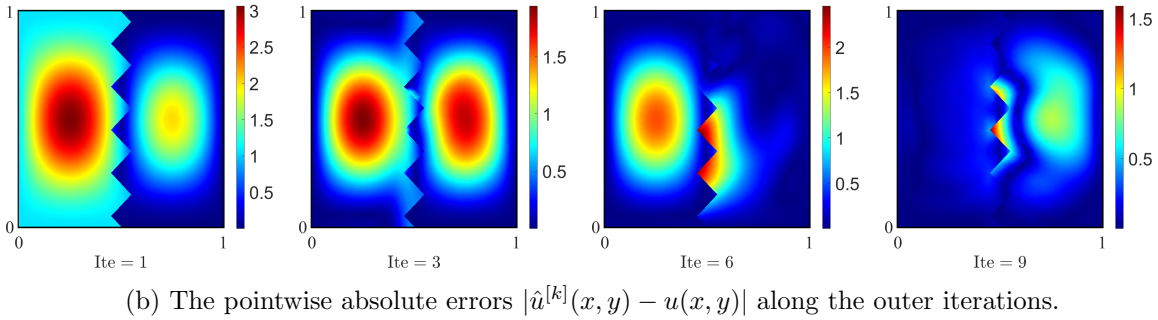
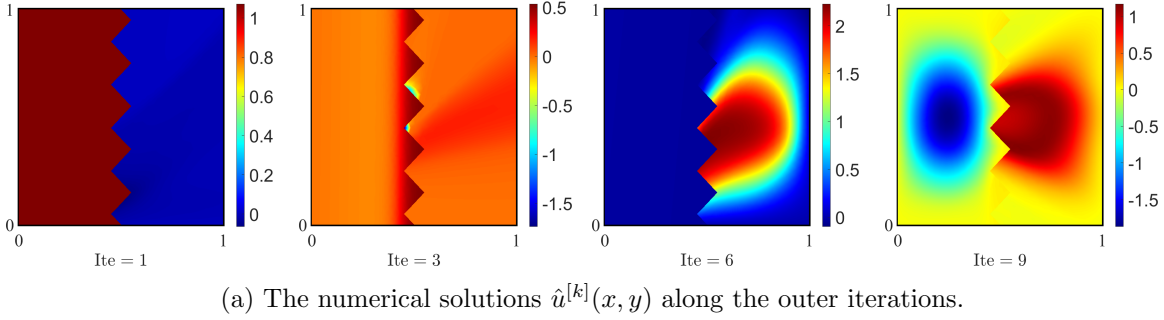
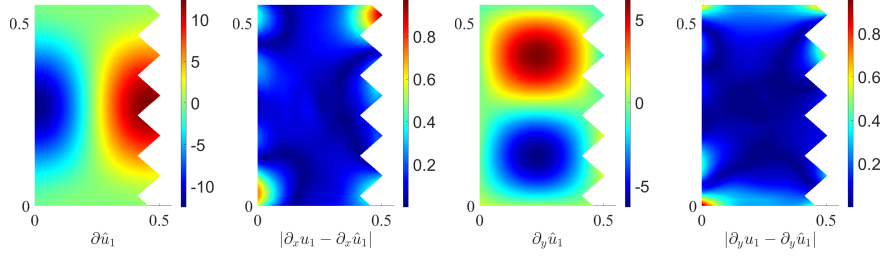
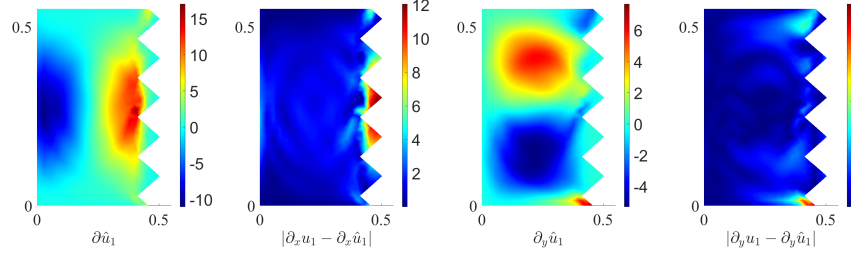


Figure 12: Numerical results of example (5.2) using our DNLM (deep Ritz) on the test dataset.



(a) Network solutions $\partial_x \hat{u}_1^{[4]}$, $\partial_y \hat{u}_1^{[4]}$ and errors $|\partial_x \hat{u}_1^{[4]} - \partial_x u_1|$, $|\partial_y \hat{u}_1^{[4]} - \partial_y u_1|$ using DNLM (PINN).



(b) Network solutions $\partial_x \hat{u}_1^{[9]}$, $\partial_y \hat{u}_1^{[9]}$ and errors $|\partial_x \hat{u}_1^{[9]} - \partial_x u_1|$, $|\partial_y \hat{u}_1^{[9]} - \partial_y u_1|$ using DNLM (deep Ritz).

Figure 13: Overfitting phenomenon in solving the Dirichlet subproblem of (5.2) on testdata.

Table 2: Relative L_2 errors of the predicted solution along the outer iteration k for example (5.2), with mean value (\pm standard deviation) being reported over 5 runs.

Outer Iterations		1	2	3	4	5
Relative Errors						
$\frac{\ \hat{u}^{[k]} - u\ _{L_2(\Omega)}}{\ u\ _{L_2(\Omega)}}$	DN-PINNs	3.12 (± 1.18)	1.92 (± 0.95)	1.69 (± 0.58)	1.77 (± 0.32)	1.70 (± 0.19)
	DNLM (PINN)	1.49 (± 0.43)	0.95 (± 0.39)	0.30 (± 0.28)	0.27 (± 0.26)	0.38 (± 0.36)
	DNLM (Deep Ritz)	1.64 (± 0.45)	1.37 (± 0.14)	1.39 (± 0.08)	1.40 (± 0.02)	1.40 (± 0.01)

where true solution $u(x, y) = \sin(2\pi x)(\cos(2\pi y) - 1) + 100xy(x - 1)^2(y - 1)^2$, and $f(x, y) = 4\pi^2 \sin(2\pi x)(2\cos(2\pi y) - 1) - 200x(x - 1)^2(3y - 2) - 200y(y - 1)^2(3x - 2)$. Here the domain is decomposed using the red-black partition [45], and the multidomains are categorized into two sets [45] as depicted in Figure 15. Then, the learning algorithms of interest can be deployed, and the initial guess of Dirichlet data along the interface is chosen as

$$h^{[0]}(x, y) = u(x, y) - 50x(x - 1)y \quad \text{on } \Gamma.$$

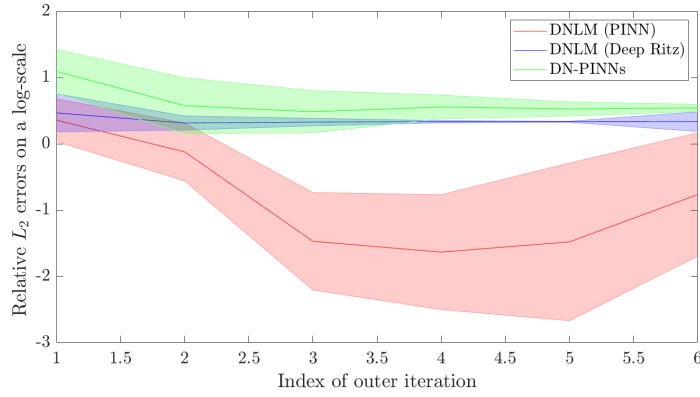


Figure 14: Relative L_2 errors on testdata along outer iterations for example (5.2).

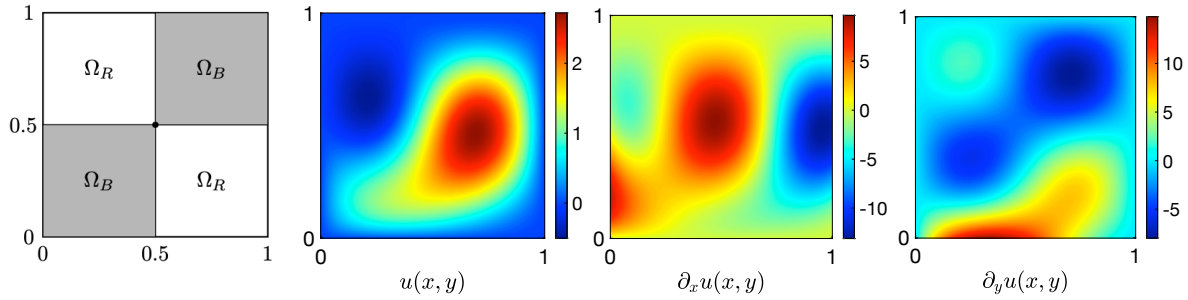


Figure 15: From left to right: decomposition of domain into two subregions, exact solution $u(x, y)$ and its partial derivatives $\partial_x u(x, y)$, $\partial_y u(x, y)$ for numerical example (5.3).

For the more general multidomain problem (5.3) with non-trivial flux functions, the numerical results using DN-PINNs are depicted in Figure 16, which is not guaranteed to converge to the true solution due to the issue of interface overfitting.

Note that the overfitting phenomenon on subdomain interfaces remains unsettled when using our methods (see Figure 19). However, thanks to the compensated deep Ritz method, it can be observed from Figure 17 and Figure 18 that the outer iterations using DNLM (PINN) and DNLM (deep Ritz) have converged, which validates the effectiveness of our proposed methods in dealing with the inevitable overfitting problem in practice. Moreover, we execute the simulation for 5 runs and report the statistical results in Table 3 and Figure 20 to further demonstrate that DNLM (PINN) can outperform other methods in terms of accuracy.

5.1.4. Poisson's Equation in High Dimension. As is well known, another key and desirable advantage of using deep learning solvers is that it can tackle difficulties induced by the

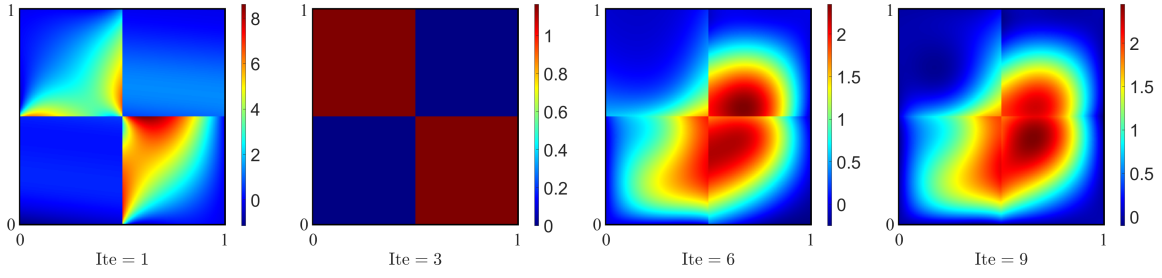
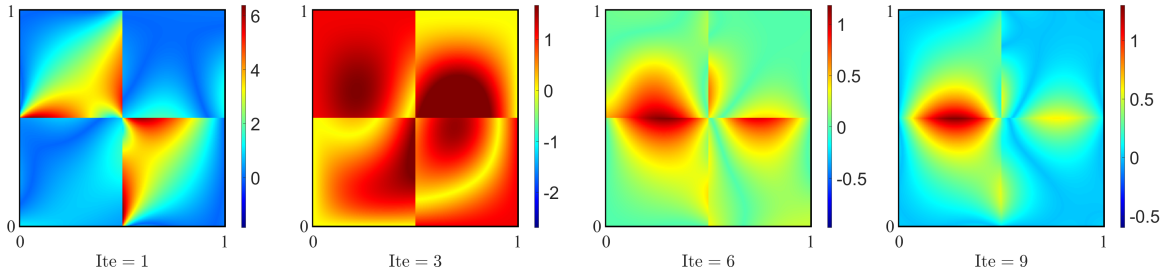
(a) The numerical solutions $\hat{u}^{[k]}(x, y)$ along the outer iterations.(b) The pointwise absolute errors $|\hat{u}^{[k]}(x, y) - u(x, y)|$ along the outer iterations.

Figure 16: Numerical results of example (5.3) using the DN-PINNs on the test dataset.

Table 3: Relative L_2 errors of the predicted solution along the outer iteration k for example (5.3), with mean value (\pm standard deviation) being reported over 5 runs.

Outer Iterations		1	2	3	4	6
Relative Errors						
$\frac{\ \hat{u}^{[k]} - u\ _{L_2(\Omega)}}{\ u\ _{L_2(\Omega)}}$	DN-PINNs	2.40 (± 0.13)	1.49 (± 0.22)	0.82 (± 0.13)	0.91 (± 0.52)	0.58 (± 0.18)
	DNLM (PINN)	1.68 (± 0.16)	1.30 (± 0.24)	0.88 (± 0.26)	0.35 (± 0.11)	0.29 (± 0.28)
	DNLM (Deep Ritz)	1.97 (± 0.47)	1.38 (± 0.29)	0.90 (± 0.29)	0.95 (± 0.63)	0.42 (± 0.26)

curse of dimensionality. To this end, we consider a Poisson problem in five dimension, *i.e.*,

$$(5.4) \quad \begin{aligned} -\Delta u(x_1, \dots, x_5) &= 4\pi^2 \sum_{i=1}^5 \sin(x_i) \quad \text{in } \Omega = (0, 1)^5, \\ u(x_1, \dots, x_5) &= 0 \quad \text{on } \partial\Omega, \end{aligned}$$

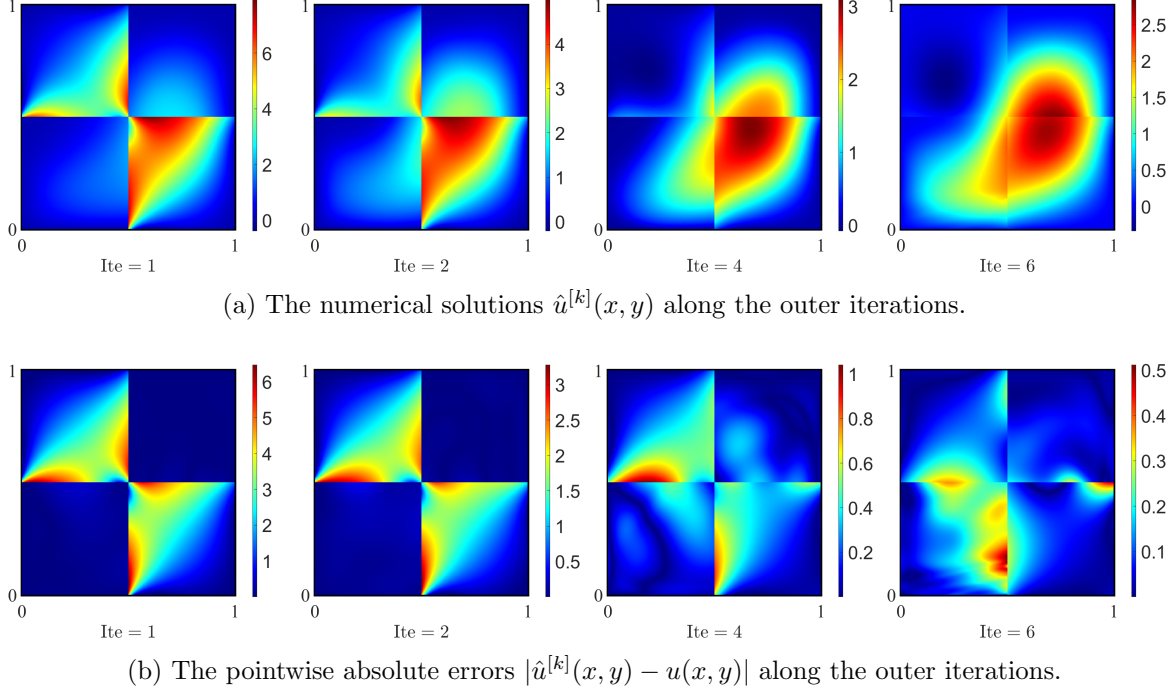


Figure 17: Numerical results of example (5.3) using our DNLM (PINN) on the test dataset.

where the exact solution is given by $u(x_1, \dots, x_5) = \sum_{i=1}^5 \sin(x_i)$, and the domain is decomposed into two subregions

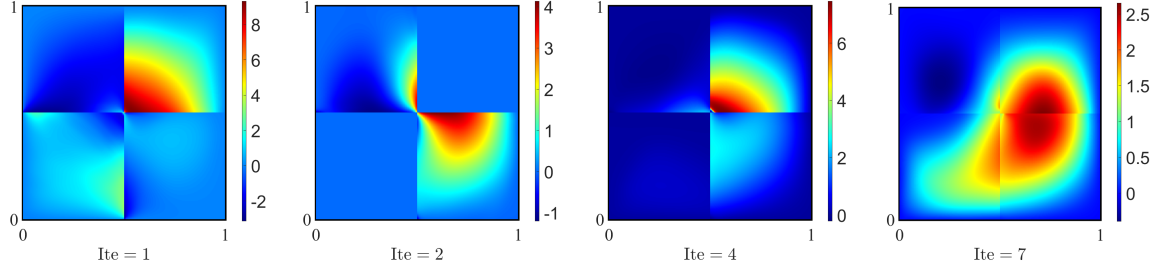
$$\Omega_1 = \{(x_1, \dots, x_5) \in \Omega \mid x_1 < 0.5\} \quad \text{and} \quad \Omega_2 = \{(x_1, \dots, x_5) \in \Omega \mid x_1 > 0.5\}.$$

Here, the initial guess of the Dirichlet data at interface is chosen as

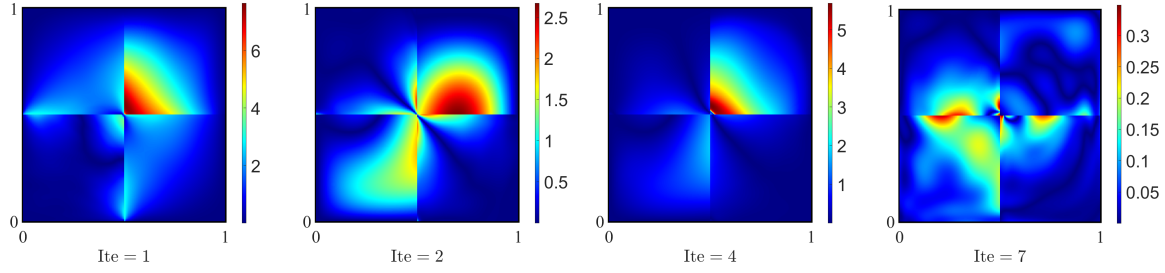
$$h^{[0]}(\mathbf{x}) = -5000 \sum_{i=1}^5 \prod_{i=1}^5 x_i (x_i - 1),$$

and the fully-connected neural network employed here has 4 hidden layers of 50 neurons each. The computational results using DN-PINNs, DNLM (PINN), and DNLM (Deep Ritz) approaches are shown in Table 4 and Figure 21, which implies that our proposed learning algorithms can achieve comparable performance to the existing learning methods.

5.1.5. High-Contrast Elliptic Equation. Note that as mentioned in remark 4.1, our proposed Dirichlet-Neumann learning algorithm 4.1 can also be easily extended to solving the more complicated interface problems with high-contrast coefficients. As such, we consider the

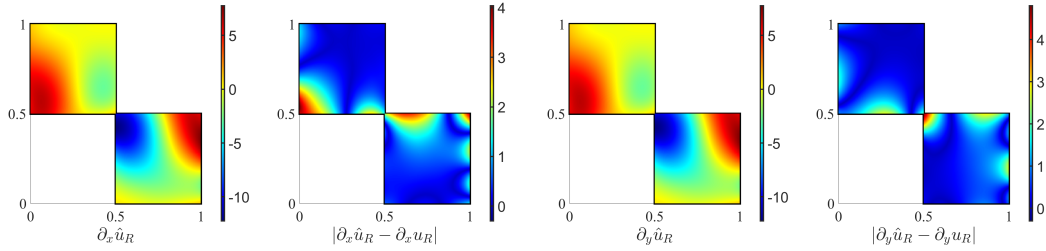


(a) The numerical solutions $\hat{u}^{[k]}(x, y)$ along the outer iterations.

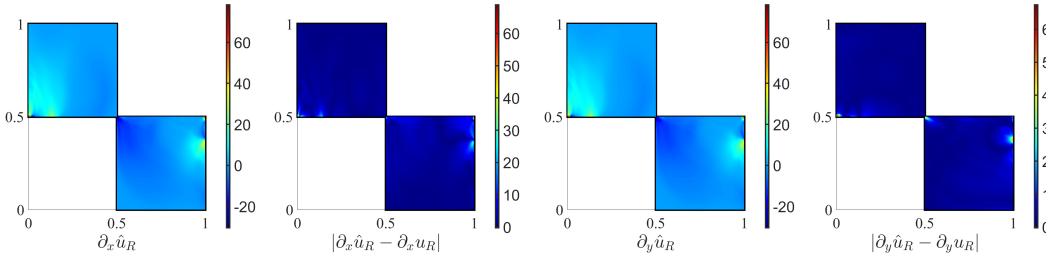


(b) The pointwise absolute errors $|\hat{u}^{[k]}(x, y) - u(x, y)|$ along the outer iterations.

Figure 18: Numerical results of example (5.3) using our DNLM (deep Ritz) on the test dataset.



(a) Network solutions $\partial_x \hat{u}_R^{[6]}$, $\partial_y \hat{u}_R^{[6]}$ and errors $|\partial_x \hat{u}_R^{[6]} - \partial_x u_R|$, $|\partial_y \hat{u}_R^{[6]} - \partial_y u_R|$ using DNLM (PINN).



(b) Network solutions $\partial_x \hat{u}_R^{[7]}$, $\partial_y \hat{u}_R^{[7]}$ and errors $|\partial_x \hat{u}_R^{[7]} - \partial_x u_R|$, $|\partial_y \hat{u}_R^{[7]} - \partial_y u_R|$ using DNLM (deep Ritz).

Figure 19: Overfitting phenomenon in solving the Dirichlet subproblem of (5.3) on testdata.

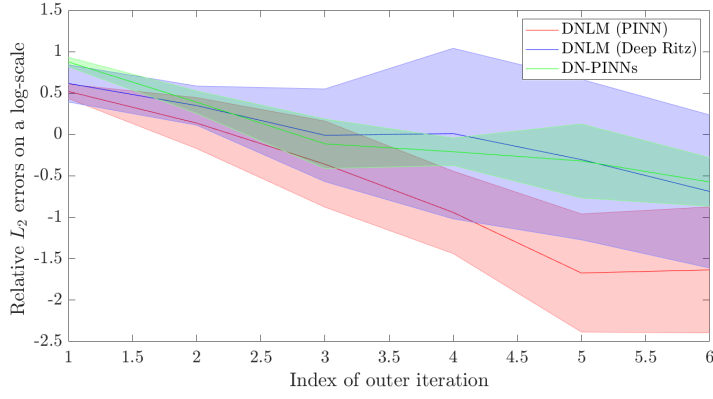


Figure 20: Relative L_2 errors on testdata along outer iterations for example (5.3).

Table 4: Relative L_2 errors of the predicted solution along the outer iteration k for example (5.4), with mean value (\pm standard deviation) being reported over 5 runs.

Outer Iterations		1	3	5	7
Relative Errors					
$\frac{\ \hat{u}^{[k]} - u\ _{L_2(\Omega)}}{\ u\ _{L_2(\Omega)}}$	DN-PINNs	0.77 (± 0.38)	0.08 (± 0.12)	0.01 (± 0.06)	0.02 (± 0.03)
	DNLM (PINN)	0.48 (± 0.03)	0.04 (± 0.01)	0.05 (± 0.02)	0.05 (± 0.02)
	DNLM (Deep Ritz)	0.54 (± 0.80)	0.11 (± 0.11)	0.05 (± 0.02)	0.04 (± 0.02)

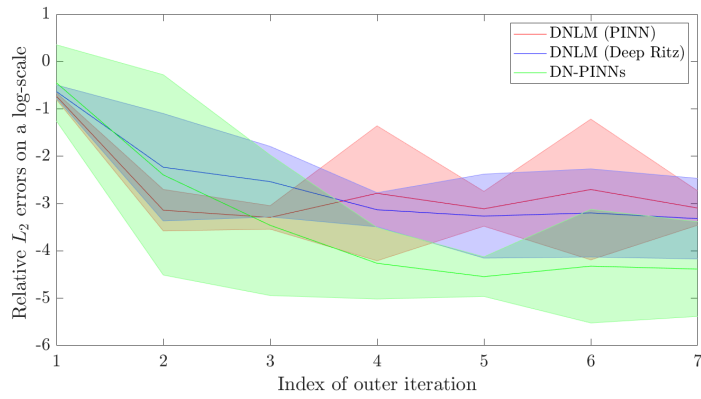


Figure 21: Relative L_2 errors on testdata along outer iterations for example (5.4).

an elliptic interface problem in two dimension, that is,

$$(5.5) \quad \begin{aligned} -\nabla \cdot (c(x, y) \nabla u(x, y)) &= 32\pi^2 \sin(4\pi x) \cos(4\pi y) & \text{in } \Omega = (0, 1)^2, \\ u(x, y) &= 0 & \text{on } \partial\Omega, \end{aligned}$$

where the domain is decomposed into four subregions using the red-black partition (see Figure 22), the exact solution is given by $u(x, y) = \sin(4\pi x) \sin(4\pi y)/c(x, y)$, and the coefficient $c(x, y)$ is piecewise constant with respect to the partition of domain

$$c(x, y) = \begin{cases} 1 & \text{in } \Omega_R, \\ 100 & \text{in } \Omega_B. \end{cases}$$

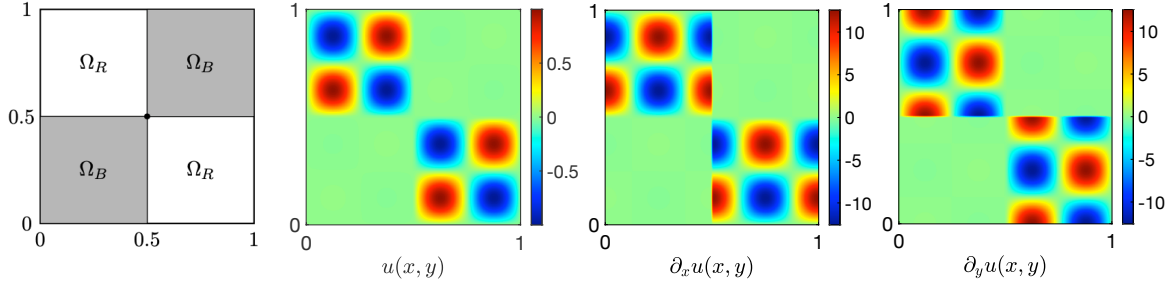


Figure 22: From left to right: decomposition of domain into two subregions, exact solution $u(x, y)$ and its partial derivatives $\partial_x u(x, y)$, $\partial_y u(x, y)$ for numerical example (5.5).

Here, we choose $h^{[0]} = 100 \cos(100\pi x) \cos(100\pi y) + 100xy(x-1)^3(y-1)^3$ as the initial guess on the interface, and the computational results using DN-PINNs, DNLM (PINN), and DNLM (deep Ritz) are depicted in Figure 23, Figure 24, and Figure 25, respectively. Clearly, our proposed learning methods can facilitate the convergence of outer iteration with guaranteed accuracy than the straightforward DN-PINNs approach, which shows the potential to solve more complicated interface problems in the presence of interface overfitting (see Figure 26).

Moreover, the statistical results over 5 runs are reported in Table 5 and Figure 27, which further validate the effectiveness of our proposed learning methods for solving the elliptic interface problems.

5.2. Robin-Robin Learning method. To demonstrate the effectiveness and efficiency of our compensated deep Ritz method for realizing the classical Robin-Robin algorithm, we consider the following Poisson equation in two-dimension

$$(5.6) \quad \begin{aligned} -\Delta u(x, y) &= 4\pi^2 \sin(2\pi x) (2 \cos(2\pi y) - 1) & \text{in } \Omega = (0, 1)^2, \\ u(x, y) &= 0 & \text{on } \partial\Omega, \end{aligned}$$

where the exact solution $u(x, y) = \sin(2\pi x)(\cos(2\pi y) - 1)$, and the interface $\Gamma = \partial\Omega_1 \cap \partial\Omega_2$ is a straight line segment from $(0.5, 0)$ to $(0.5, 1)$ as depicted in Figure 3.

By choosing $(\kappa_1, \kappa_2) = (1, 0.01)$, the computational results using RR-PINNs, *i.e.*, Algorithm 3.1, in a typical simulation is depicted Figure 28, which can converge to the true

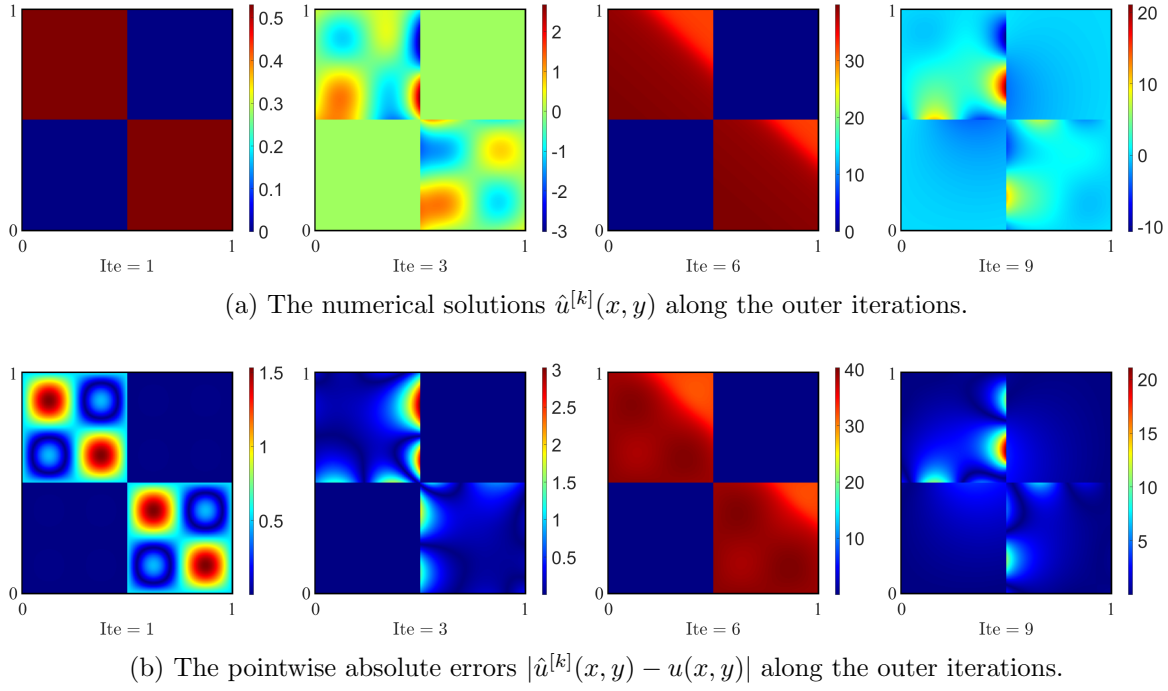


Figure 23: Numerical results of example (5.5) using the DN-PINNs on the test dataset.

Table 5: Relative L_2 errors of the predicted solution along the outer iteration k for example (5.5), with mean value (\pm standard deviation) being reported over 5 runs.

Outer Iterations		1	3	5	6	7
Relative Errors						
$\frac{\ \hat{u}^{[k]} - u\ _{L_2(\Omega)}}{\ u\ _{L_2(\Omega)}}$	DN-PINNs	1.90 (± 1.03)	1.17 (± 0.34)	13.75 (± 22.70)	20.19 (± 33.04)	2.47 (± 2.45)
	DNLM (PINN)	62.46 (± 56.64)	0.92 (± 0.31)	0.65 (± 0.49)	0.83 (± 0.40)	0.51 (± 0.54)
	DNLM (Deep Ritz)	81.56 (± 48.50)	0.98 (± 0.14)	2.94 (± 4.41)	4.72 (± 8.80)	0.82 (± 0.42)

solution but requires more outer iterations when compared to the DNLM (PINN) or DNLM (deep Ritz) approach (see Figure 5 or Figure 6).

To further enhance the speed of outer convergence, these two additional parameters are set to be $(\kappa_1, \kappa_2) = (1, 1000)$ in what follows. Unfortunately, due to the weights imbalance, the RR-PINNs approach could not work under such a circumstance (see Figure 30). On the other hand, the integration with our compensated deep Ritz method (see Figure 29 and Figure 31) is convergent in the presence of interface overfitting, which only requires the substitution of

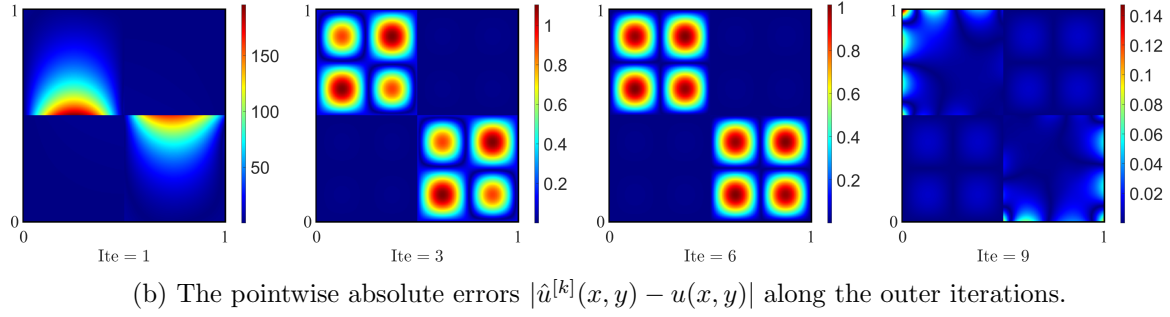
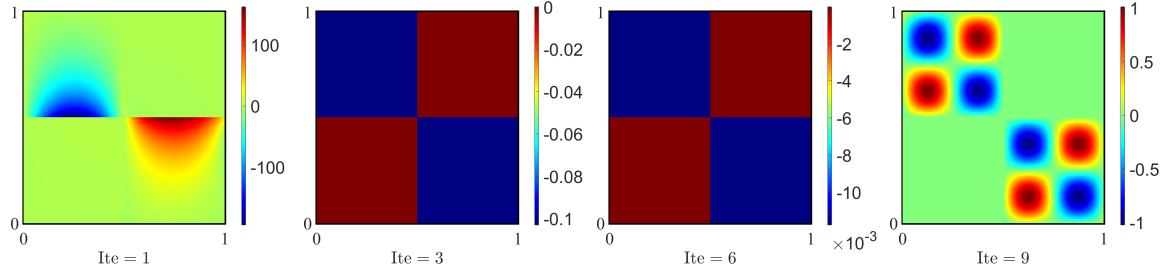


Figure 24: Numerical results of example (5.5) using our DNLM (PINN) on the test dataset.

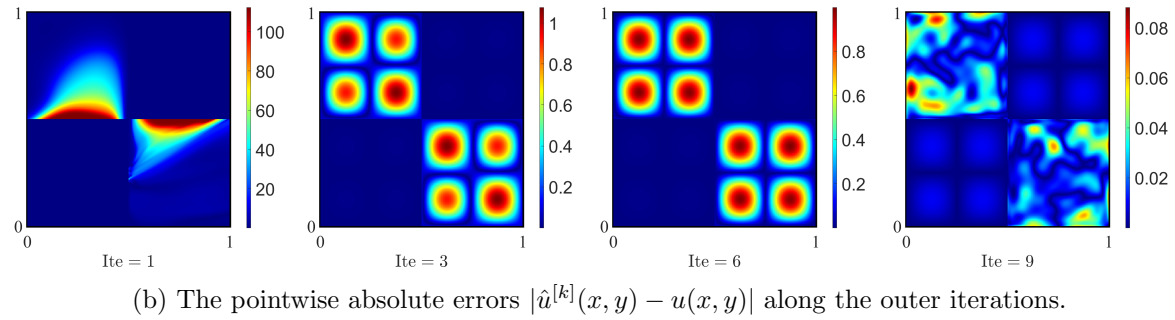
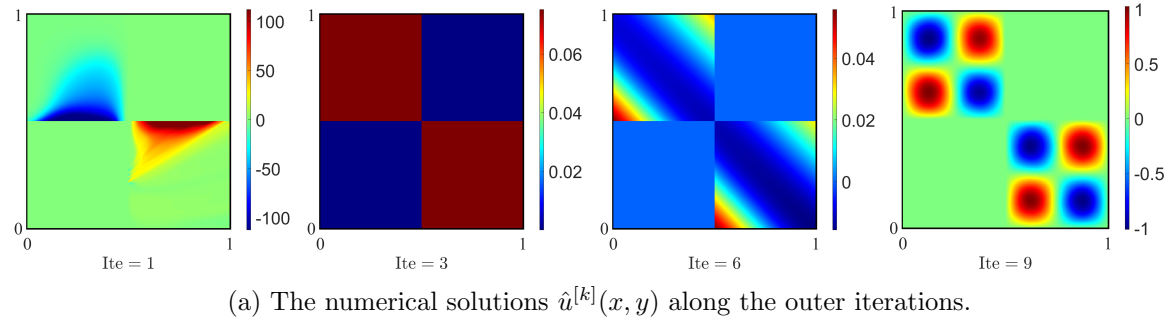


Figure 25: Numerical results of example (5.5) using our DNLM (deep Ritz) on the test dataset.

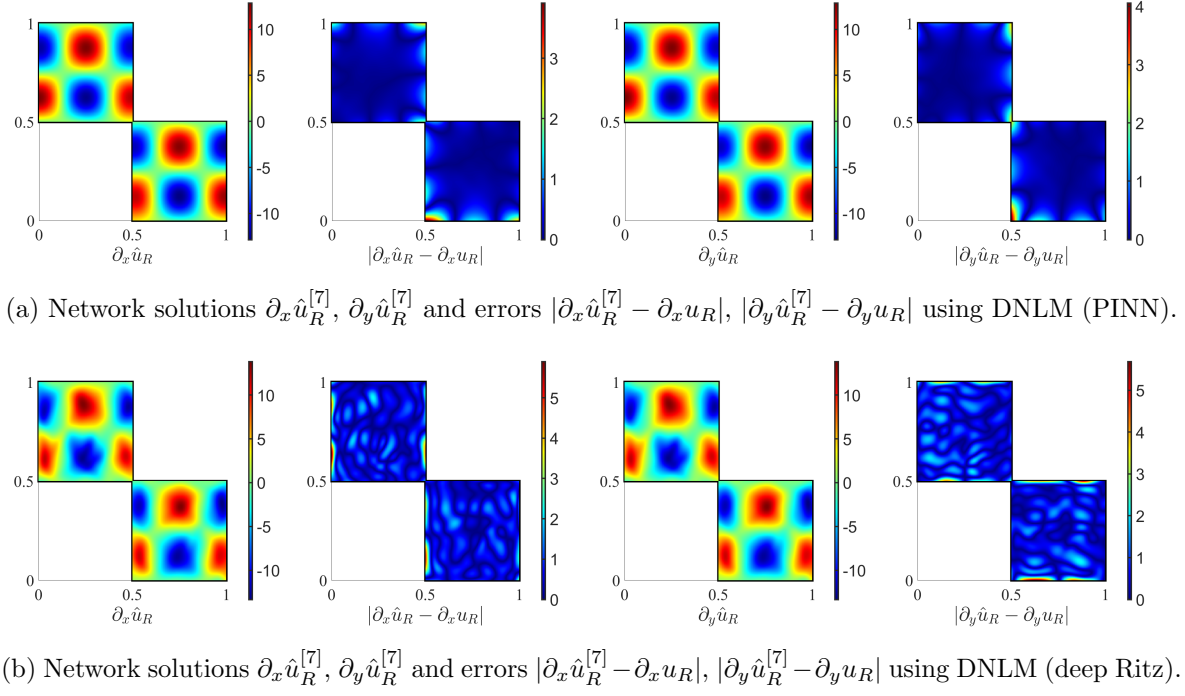


Figure 26: Overfitting phenomenon in solving the Dirichlet subproblem of (5.5) on testdata.

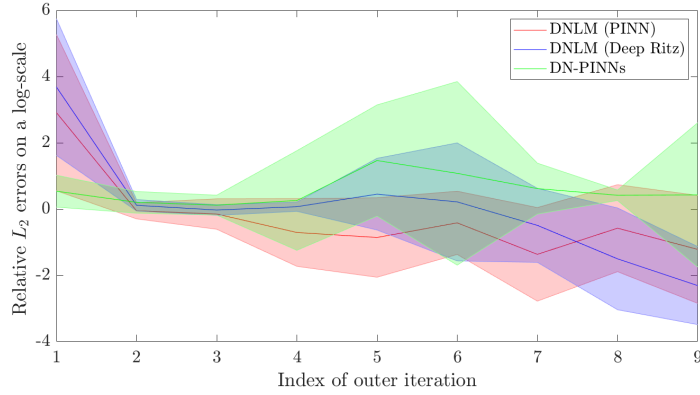


Figure 27: Relative L_2 errors on testdata along outer iterations for example (5.4).

second subproblem with our proposed learning approach.

6. Conclusion. In this paper, a general framework is proposed for realizing the classical domain decomposition methods through deep learning approaches, which is based on the information exchange between neighbouring subregions rather than the domain partition strategies. For the methods that are based on a direct flux exchange, a key difficulty of deploying the deep

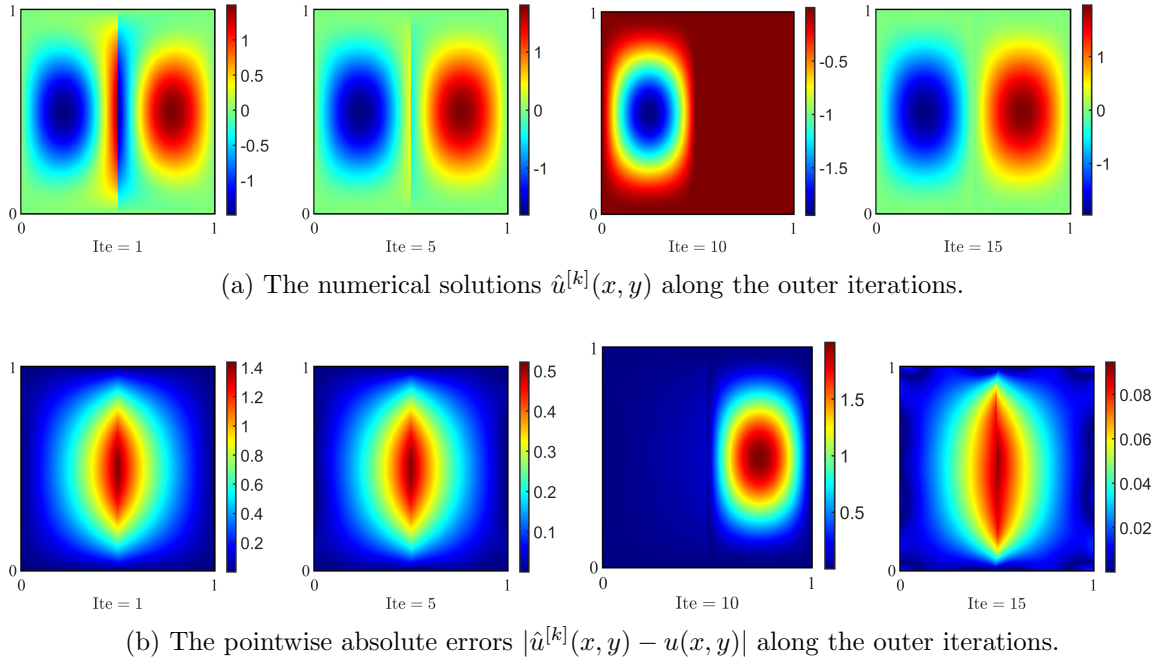


Figure 28: Numerical results of example (5.6) using the RR-PINNs on the test dataset.

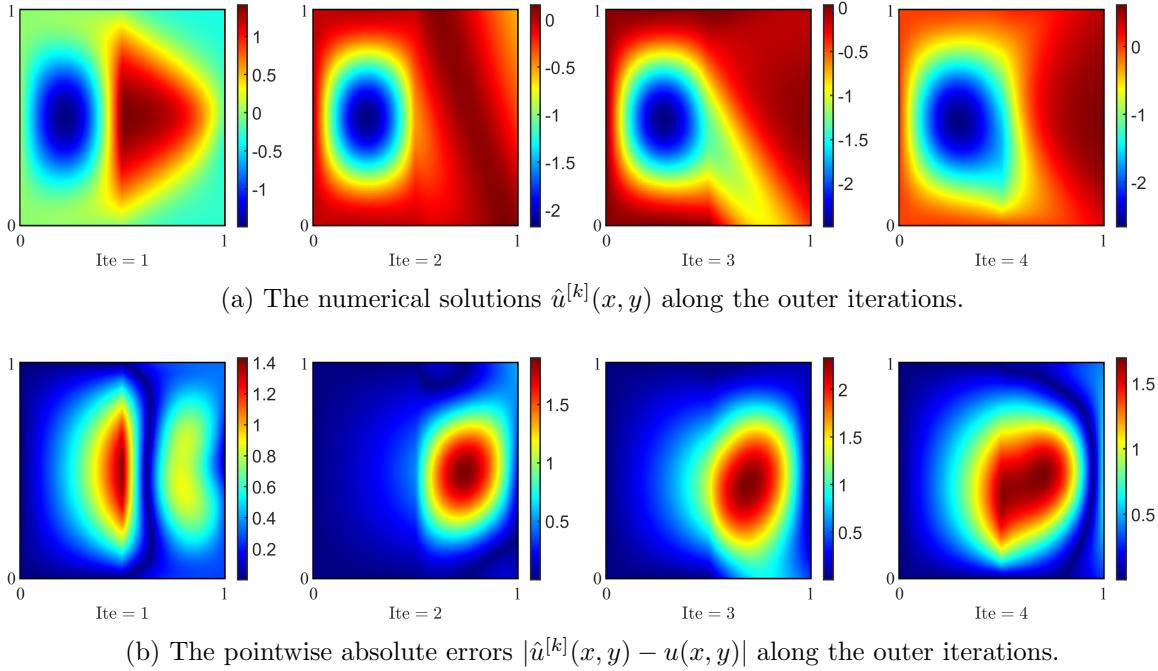
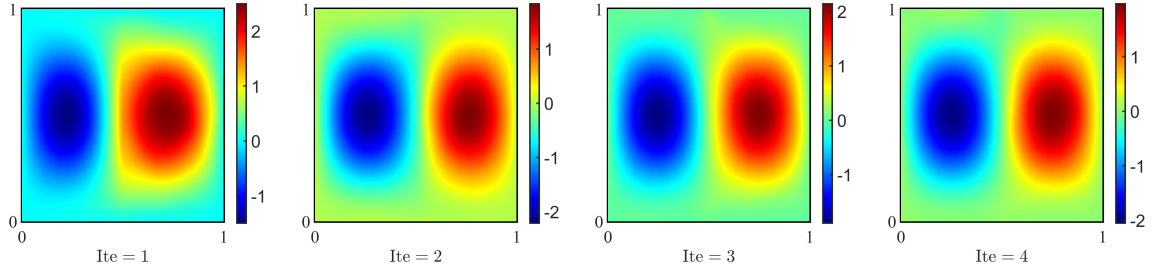
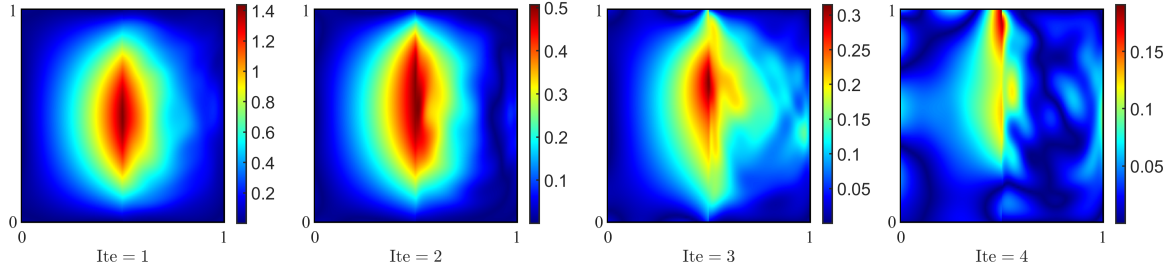


Figure 29: Numerical results of example (5.6) using the RR-PINNs on the test dataset.

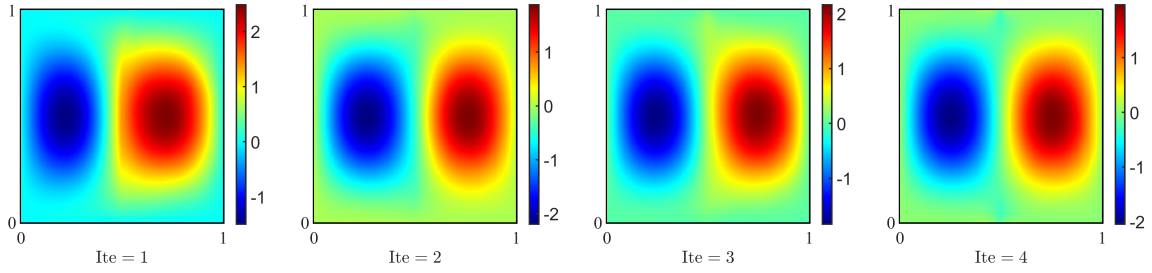


(a) The numerical solutions $\hat{u}^{[k]}(x, y)$ along the outer iterations.

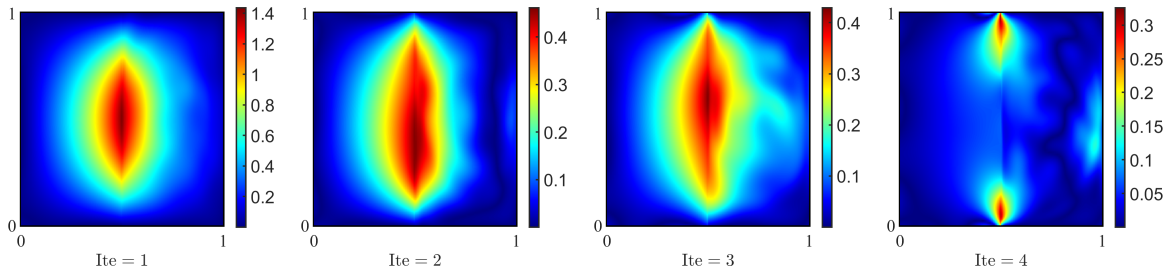


(b) The pointwise absolute errors $|\hat{u}^{[k]}(x, y) - u(x, y)|$ along the outer iterations.

Figure 30: Numerical results of example (5.6) using our RRLM (PINN) on the test dataset.



(a) The numerical solutions $\hat{u}^{[k]}(x, y)$ along the outer iterations.



(b) The pointwise absolute errors $|\hat{u}^{[k]}(x, y) - u(x, y)|$ along the outer iterations.

Figure 31: Numerical results of example (5.6) using our RRLM (deep Ritz) on the test dataset.

learning solvers is the issue of interface overfitting that will always occur to a greater or lesser extent in practice. To deal with the overfitted interface conditions, we develop a novel learning approach, *i.e.*, the compensated deep Ritz method, that enables the flux transmission across subdomain interfaces with guaranteed accuracy. As a result, it allows us to construct effective learning approaches for realizing the classical Dirichlet-Neumann, Neumann-Neumann, and Dirichlet-Dirichlet algorithms, and therefore fully leverage the advantages of deep learning solvers to deal with the complicated geometry domains and high-dimensional problems. On the other hand, the Robin-Robin algorithm, which does not require the flux exchange but may suffer from the issue of weights imbalance, can also benefit from our compensated deep Ritz method. Finally, we conduct numerical experiments on a series of elliptic boundary value problems to demonstrate the effectiveness of our proposed learning algorithms. Possible future explorations would involve the coarse space acceleration [35], the adaptive sampling technique [14], and the improvement of network architecture that could potentially further accelerate the convergence at a reduced cost.

REFERENCES

- [1] C. BAJAJ, L. MCLENNAN, T. ANDEEN, AND A. ROY, *Robust learning of physics informed neural networks*, arXiv preprint arXiv:2110.13330, (2021).
- [2] T. BEN-NUN AND T. HOEFLER, *Demystifying parallel and distributed deep learning: An in-depth concurrency analysis*, ACM Computing Surveys (CSUR), 52 (2019), pp. 1–43.
- [3] J. BERG AND K. NYSTRÖM, *A unified deep artificial neural network approach to partial differential equations in complex geometries*, Neurocomputing, 317 (2018), pp. 28–41.
- [4] L. BOTTOU, F. E. CURTIS, AND J. NOCEDAL, *Optimization methods for large-scale machine learning*, SIAM Review, 60 (2018), pp. 223–311.
- [5] S. C. BRENNER, L. R. SCOTT, AND L. R. SCOTT, *The Mathematical Theory of Finite Element Methods*, vol. 3, Springer, 2008.
- [6] S. BRUNTON, B. NOACK, AND P. KOUMOUTSAKOS, *Machine learning for fluid mechanics*, arXiv preprint arXiv:1905.11075, (2019).
- [7] J. CHEN, R. DU, AND K. WU, *A comparison study of deep Galerkin method and deep Ritz method for elliptic problems with different boundary conditions*, arXiv preprint arXiv:2005.04554, (2020).
- [8] W. CHEN, X. XU, AND S. ZHANG, *On the optimal convergence rate of a Robin-Robin domain decomposition method*, Journal of Computational Mathematics, (2014), pp. 456–475.
- [9] T. DOCKHORN, *A discussion on solving partial differential equations using neural networks*, arXiv preprint arXiv:1904.07200, (2019).
- [10] L. C. EVANS, *Partial Differential Equations*, vol. 19, American Mathematical Society, 2010.
- [11] D. FUNARO, A. QUARTERONI, AND P. ZANOLLI, *An iterative procedure with interface relaxation for domain decomposition methods*, SIAM Journal on Numerical Analysis, 25 (1988), pp. 1213–1236.
- [12] I. GOODFELLOW, Y. BENGIO, AND A. COURVILLE, *Deep Learning*, MIT Press, 2016.
- [13] J. HAN, A. JENTZEN, ET AL., *Deep learning-based numerical methods for high-dimensional parabolic partial differential equations and backward stochastic differential equations*, Communications in Mathematics and Statistics, 5 (2017), pp. 349–380.
- [14] C. HE, X. HU, AND L. MU, *A mesh-free method using piecewise deep neural network for elliptic interface problems*, Journal of Computational and Applied Mathematics, 412 (2022), pp. 114–358.
- [15] K. HE, X. ZHANG, S. REN, AND J. SUN, *Deep residual learning for image recognition*, in Proceedings of the IEEE conference on computer vision and pattern recognition, 2016, pp. 770–778.
- [16] R. HECHT-NIELSEN, *Theory of the backpropagation neural network*, in Neural networks for perception, Elsevier, 1992, pp. 65–93.
- [17] A. HEINLEIN, A. KLAUWONN, M. LANSER, AND J. WEBER, *Combining machine learning and domain decomposition methods for the solution of partial differential equations—A review*, GAMM-Mitteilungen, 44 (2021), p. e202100001.
- [18] K. HORNIK, M. STINCHCOMBE, AND H. WHITE, *Multilayer feedforward networks are universal approximators*, Neural Networks, 2 (1989), pp. 359–366.
- [19] Z. HU, A. D. JAGTAP, G. E. KARNIAKAKIS, AND K. KAWAGUCHI, *When do extended physics-informed neural networks (XPINNs) improve generalization?*, arXiv preprint arXiv:2109.09444, (2021).
- [20] J. HUANG, H. WANG, AND T. ZHOU, *An augmented Lagrangian deep learning method for variational problems with essential boundary conditions*, arXiv preprint arXiv:2106.14348, (2021).
- [21] A. D. JAGTAP AND G. E. KARNIAKAKIS, *Extended physics-informed neural networks (XPINNs): A generalized space-time domain decomposition based deep learning framework for nonlinear partial differential equations*, Communications in Computational Physics, 28 (2020), pp. 2002–2041.
- [22] A. D. JAGTAP, E. KHARAZMI, AND G. E. KARNIAKAKIS, *Conservative physics-informed neural networks on discrete domains for conservation laws: Applications to forward and inverse problems*, Computer Methods in Applied Mechanics and Engineering, 365 (2020), pp. 113–028.
- [23] G. E. KARNIAKAKIS, I. G. KEVREKIDIS, L. LU, P. PERDIKARIS, S. WANG, AND L. YANG, *Physics-informed machine learning*, Nature Reviews Physics, 3 (2021), pp. 422–440.
- [24] I. E. LAGARIS, A. LIKAS, AND D. I. FOTIADIS, *Artificial neural networks for solving ordinary and partial differential equations*, IEEE Transactions on Neural Networks, 9 (1998), pp. 987–1000.
- [25] I. E. LAGARIS, A. C. LIKAS, AND D. G. PAPAGEORGIOU, *Neural-network methods for boundary value problems with irregular boundaries*, IEEE Transactions on Neural Networks, 11 (2000), pp. 1041–1049.

- [26] Y. LECUN, Y. BENGIO, AND G. HINTON, *Deep learning*, Nature, 521 (2015), pp. 436–444.
- [27] R. J. LEVEQUE, *Finite Difference Methods for Ordinary and Partial Differential Equations: Steady-State and Time-Dependent Problems*, SIAM, 2007.
- [28] R. J. LEVEQUE ET AL., *Finite Volume Methods for Hyperbolic Problems*, vol. 31, Cambridge University Press, 2002.
- [29] K. LI, K. TANG, T. WU, AND Q. LIAO, *D3M: A deep domain decomposition method for partial differential equations*, IEEE Access, 8 (2019), pp. 5283–5294.
- [30] W. LI, X. XIANG, AND Y. XU, *Deep domain decomposition method: Elliptic problems*, in Mathematical and Scientific Machine Learning, PMLR, 2020, pp. 269–286.
- [31] Z. LI AND K. ITO, *The Immersed Interface Method: Numerical Solutions of PDEs Involving Interfaces and Irregular Domains*, SIAM, 2006.
- [32] Y. LIAO AND P. MING, *Deep Nitsche method: Deep Ritz method with essential boundary conditions*, arXiv preprint arXiv:1912.01309, (2019).
- [33] T. MATHEW, *Domain Decomposition Methods for the Numerical Solution of Partial Differential Equations*, vol. 61, Springer Science & Business Media, 2008.
- [34] K. S. MCFALL AND J. R. MAHAN, *Artificial neural network method for solution of boundary value problems with exact satisfaction of arbitrary boundary conditions*, IEEE Transactions on Neural Networks, 20 (2009), pp. 1221–1233.
- [35] V. MERCIER, S. GRATTON, AND P. BOUDIER, *A coarse space acceleration of deep-DDM*, arXiv preprint arXiv:2112.03732, (2021).
- [36] N. METROPOLIS AND S. ULAM, *The Monte Carlo method*, Journal of the American Statistical Association, 44 (1949), pp. 335–341.
- [37] A. PASZKE, S. GROSS, S. CHINTALA, G. CHANAN, E. YANG, Z. DEVITO, Z. LIN, A. DESMAISON, L. ANTIGA, AND A. LERER, *Automatic differentiation in PyTorch*, (2017).
- [38] A. QUARTERONI AND A. VALLI, *Domain Decomposition Methods for Partial Differential Equations*, no. BOOK, Oxford University Press, 1999.
- [39] M. RAISSI, P. PERDIKARIS, AND G. E. KARNIADAKIS, *Physics-informed neural networks: A deep learning framework for solving forward and inverse problems involving nonlinear partial differential equations*, Journal of Computational physics, 378 (2019), pp. 686–707.
- [40] F. SCARSELLI AND A. C. TSOI, *Universal approximation using feedforward neural networks: A survey of some existing methods, and some new results*, Neural Networks, 11 (1998), pp. 15–37.
- [41] H. SCHWARZ, *Gesammelte mathematische abhandlungen. Vierteljahrsschrift der naturforschenden gesellschaft in Zurich*, republished by Springer-Verlag, 1870.
- [42] H. SHENG AND C. YANG, *PFNN-2: A domain decomposed penalty-free neural network method for solving partial differential equations*, arXiv preprint arXiv:2205.00593, (2022).
- [43] J. SIRIGNANO AND K. SPILIOPOULOS, *DGM: A deep learning algorithm for solving partial differential equations*, Journal of Computational Physics, 375 (2018), pp. 1339–1364.
- [44] A. TAGHIBAKHSHI, N. NYTKO, T. ZAMAN, S. MACLACHLAN, L. OLSON, AND M. WEST, *Learning interface conditions in domain decomposition solvers*, arXiv preprint arXiv:2205.09833, (2022).
- [45] A. TOSELLI AND O. WIDLUND, *Domain Decomposition Methods: Algorithms and Theory*, vol. 34, Springer Science & Business Media, 2004.
- [46] C. L. WIGHT AND J. ZHAO, *Solving Allen-Cahn and Cahn-Hilliard equations using the adaptive physics informed neural networks*, arXiv preprint arXiv:2007.04542, (2020).
- [47] B. YU ET AL., *The deep Ritz method: a deep learning-based numerical algorithm for solving variational problems*, Communications in Mathematics and Statistics, 6 (2018), pp. 1–12.
- [48] Y. ZANG, G. BAO, X. YE, AND H. ZHOU, *Weak adversarial networks for high-dimensional partial differential equations*, Journal of Computational Physics, 411 (2020), pp. 109–409.